

QoS-based Beamforming and Compression Design for Cooperative Cellular Networks via Lagrangian Duality

Xilai Fan, Ya-Feng Liu, Liang Liu, and Tsung-Hui Chang

Abstract—This paper considers the quality-of-service (QoS)-based joint beamforming and compression design problem in the downlink cooperative cellular network, where multiple relay-like base stations (BSs), connected to the central processor via rate-limited fronthaul links, cooperatively transmit messages to the users. The problem of interest is formulated as the minimization of the total transmit power of the BSs, subject to all users' signal-to-interference-plus-noise ratio (SINR) constraints and all BSs' fronthaul rate constraints. In this paper, we first show that there is no duality gap between the considered joint optimization problem and its Lagrangian dual by showing the tightness of its semidefinite relaxation (SDR). Then, we propose an efficient algorithm based on the above duality result for solving the considered problem. The proposed algorithm judiciously exploits the special structure of an enhanced Karush-Kuhn-Tucker (KKT) conditions of the considered problem and finds the solution that satisfies the enhanced KKT conditions via two fixed point iterations. Two key features of the proposed algorithm are: (1) it is able to detect whether the considered problem is feasible or not and find its globally optimal solution when it is feasible; (2) it is highly efficient because both of the fixed point iterations in the proposed algorithm are linearly convergent and evaluating the functions in the fixed point iterations are computationally cheap. Numerical results show the global optimality and efficiency of the proposed algorithm.

Index Terms—Cooperative cellular network, enhanced Karush-Kuhn-Tucker (KKT) conditions, fixed point iteration, Lagrangian duality, tightness of semidefinite relaxation (SDR).

I. INTRODUCTION

LAGRANGIAN duality [2], a principle that (convex) optimization problems can be viewed from either the primal or the dual perspective, is a powerful and vital tool in revealing the intrinsic structures of the optimization problems arising from engineering and further better solving the problems. In practical engineering design, one is often interested in not only the numerical solution to the corresponding problems but also the specific structure of their optimal solutions. When a problem is formulated as a convex optimization problem,

exploring its Lagrangian dual often reveals such structure. Knowing these solution structures in turn often leads to a better algorithm for solving the corresponding problem.

The celebrated uplink-downlink duality [3]–[7] in the power control and beamforming design literature can be comprehensively understood and interpreted by Lagrangian duality [8], [9]. The uplink-downlink duality refers to the fact that the minimum sum power required to achieve a set of signal-to-interference-plus-noise ratio (SINR) targets in the downlink channel is equal to that to achieve the same set of SINR targets in a virtual dual uplink channel, when the uplink and downlink channels are the conjugate transpose of each other. Usually, the virtual uplink beamforming problems, e.g., the sum transmission power minimization problems subject to users' SINR constraints, can be derived from some equivalent transformation of the Lagrangian dual of the downlink problem [8] and solved globally and efficiently via the fixed point iteration algorithm [3], [6], [10], [11]. The uplink-downlink duality thus enables efficient algorithms for solving the downlink problem via solving the relatively easy uplink (essentially dual) counterpart. This line of algorithms enjoys two key features: one is its high computational efficiency as the algorithm often only involves very cheap fixed point iterations, and the other is its global optimality. Indeed, the Lagrangian duality and in particular the uplink-downlink duality based algorithms have been widely studied for solving power control and beamforming design problems in various communication networks; see [3]–[18] and the references therein.

Different from the above works where the degree of the cooperation between the base stations (BSs) is limited, this paper considers the cooperative cellular network where the users' data information are shared among the BSs via the fronthaul links and the joint processing is performed at the central processor (CP), which can effectively mitigate the inter-cell interference. Such network includes coordinated multipoint [19], distributed antenna system [20], cloud radio access network (C-RAN) [21], and cell-free massive multi-input multi-output [22] as special cases. Despite the attractive advantages of full cooperation between the BSs, the cooperative cellular network puts heavy burden on the required fronthaul links. To tackle the above issue, transmission strategies of the BSs should be jointly designed along with the utilization of the fronthaul links [23]. Along this direction, a variety of solutions have been proposed under different design objectives and system settings; see [24]–[38] and the references therein.

However, very few of the above works have exploited

Part of this work has been presented at the IEEE International Conference on Acoustics, Speech, and Signal Processing (ICASSP) 2022 [1]. X. Fan and Y.-F. Liu are with the State Key Laboratory of Scientific and Engineering Computing, Institute of Computational Mathematics and Scientific/Engineering Computing, Academy of Mathematics and Systems Science, Chinese Academy of Sciences, Beijing 100190, China (e-mail: {fanxilai, yafliu}@lsec.cc.ac.cn). L. Liu is with the Department of Electronic and Information Engineering, The Hong Kong Polytechnic University, Hong Kong SAR, China (e-mail: liang-eie.liu@polyu.edu.hk). T.-H. Chang is with the School of Science and Engineering, The Chinese University of Hong Kong, Shenzhen, Shenzhen, China, and Shenzhen Research Institute of Big Data (e-mail: tsunghui.chang@ieee.org).

the Lagrangian duality or uplink-downlink duality in the cooperative cellular network (possibly due to the reason that the optimization problem therein seems to be nonconvex). The goal of this paper is to fill this gap, i.e., exploiting the Lagrangian duality in the joint beamforming and compression design problem in the cooperative cellular network to reveal its special solution structure and utilize them to develop efficient algorithms.

A. Prior Works

Duality-based algorithms for the downlink beamforming problem in the conventional cellular network have been studied extensively in [5], [6], [15]–[17]. Assuming single-antenna users, a multi-antenna BS, and linear encoding and decoding strategies employed at the BS, the works in [3]–[8] showed that any downlink achievable SINR tuple can be achieved in the uplink under the same sum power constraint, and vice versa. Such uplink-downlink duality results enable efficient algorithms for solving the downlink beamforming problem. More specifically, the work [5] proposed an alternating optimization algorithm for solving the downlink beamforming problem and showed the global optimality of the algorithm. Instead of exactly solving the power allocation subproblem as in [5], [6] proposed efficient fixed point algorithms for solving the downlink beamforming problem. Using the nonlinear Perron-Frobenius theory [39], the work [15] proved that the fixed point iteration algorithm proposed in [6] is guaranteed to find the global solution. In addition, there have been works that exploit the uplink-downlink duality for downlink beamforming problems under various practical constraints, such as per-antenna power constraints [16] and indefinite shaping constraints [17].

In the cooperative cellular networks, the joint beamforming and compression problem, i.e., the joint design of the wireless transmission and the compression-based utilization of the fronthaul links, has been widely studied under various designing criteria and system settings [26]–[29], [31], [33]–[38]. To fully utilize fronthaul links of finite capacities, an information-theoretically optimal compression strategy called multivariate compression was proposed in [26]. Refs. [26] and [27] studied the joint design of the beamformer and the covariance of the quantization noise under the assumption that the CP adopts the linear encoding strategy and the multivariate compression strategy to compress the signals before transmitting them to the relay-like BSs. More specifically, Ref. [26] considered the weighted sum rate maximization problem with the total transmission power constraint at the CP and the fronthaul rate constraints of all relay-like BSs and proposed a successive convex approximation (SCA) algorithm for solving the considered problem. Ref. [27] further extended the above joint beamforming and compression design problem to the multi-cluster C-RAN case (with multiple CPs).

In contrast to beamforming problems in conventional cellular networks, there is a scarcity of duality results and duality-based algorithms for the design of joint beamforming and compression in cooperative cellular networks. Indeed, most of the existing works use non-convex optimization techniques

(e.g., SCA) to tackle the joint beamforming and compression design problems in the cooperative cellular network. Recently, Refs. [40] and [41] generalized the uplink-downlink duality result from the conventional cellular network to the cooperative cellular network. Additionally, [41] formulated a QoS-based joint beamforming and compression design problem and proposed an algorithm for solving it based on the established duality result. The algorithm in [41] first obtains the optimal downlink beamformers by solving the uplink problem via fixed point iterations and then solves the downlink joint power control and compression problem with fixed beamformers.

B. Our Contributions

In this paper, we consider the same QoS-based joint beamforming and compression design problem (see problem (2) further ahead) as in [41] but make further progress in developing the duality result and designing the duality-based algorithm. The main contributions of this paper are twofold.

- *New Lagrangian Duality Result.* We establish the tightness of the semidefinite relaxation (SDR) of the considered problem and thus the equivalence of the two problems. This result further implies that the dual problem of the considered problem and its SDR are the same. This Lagrangian duality result significantly facilitates the algorithmic design and plays a central role in the proposed algorithm for solving the problem. Our duality result is sharply different from the established duality result in [41], where the problem (2) with fixed beamformers is considered. The problem (2) with fixed beamformers is already in a convex form (after some algebraic manipulation), while the problem (2) itself is not, and whether it admits a convex reformulation is an open question in [41, Section IX-B]. This makes our Lagrangian duality result nontrivial.
- *Efficient Fixed Point Iteration Algorithm.* Based on the established duality result, we propose an efficient algorithm for solving the SDR of the considered problem. The basic idea of the proposed algorithm is to solve the enhanced Karush-Kuhn-Tucker (KKT) conditions, which incorporate the special structures of the problem into the classical KKT conditions. In particular, the proposed algorithm first solves the enhanced KKT conditions involving the dual variables via a fixed point iteration and then solves the enhanced KKT conditions involving the primal variables via another fixed point iteration. Two key features of the proposed algorithm are as follows: (1) it is guaranteed to find the global solution of the problem when it is feasible and is able to detect the infeasibility of the problem when it is not; (2) it is highly efficient because both fixed point iterations in the proposed algorithm enjoy linear convergence rates, and each update of the variables in fixed point iterations is computationally cheap. The proposed algorithm leverages more Lagrangian duality relationship as compared with that in [41]. In particular, after obtaining the dual variables, our algorithm recovers the primal variables (e.g., power control vector and compression covariance matrix)

via the fixed point iteration. This is different from the algorithm in [41], which requires solving the downlink joint power control and compression problem with fixed beamformers from scratch. This key difference is due to the new Lagrangian duality result and makes our proposed algorithm significantly outperform the algorithm in [41] in terms of the computational efficiency.

In our prior work [1], we presented an efficient fixed point iteration algorithm for solving the QoS-based joint beamforming and compression design problem. The present paper, however, is a significant extension of [1]. First, we provide crucial details on the convergence proof of the fixed point iterations, which were missing in our prior work. Second, we show the linear convergence rate of the proposed fixed point iteration algorithm and study the behaviors of the proposed algorithm when the considered problem is infeasible. These theoretical results are completely new compared with our prior work. Third, we conduct detailed numerical experiments that compare the proposed algorithm with the state-of-the-art (SOTA) benchmarks.

C. Organization

We adopt the following notations in this paper. We use \mathcal{S}_+^n to denote the set of all $n \times n$ positive definite matrices, \mathcal{S}_+^n to denote the set of all $n \times n$ positive semidefinite matrices, \mathbb{R}_+^n to denote the n -dimensional positive orthant, and \mathbb{R}_+^n to denote the n -dimensional non-negative orthant. The order relationship between two vectors shall be understood component-wise. For any matrix \mathbf{A} , \mathbf{A}^\dagger and \mathbf{A}^\top denote the conjugate transpose and transpose of \mathbf{A} , respectively; $\mathbf{A}^{(m,n)}$ denotes the entry on the m -th row and the n -th column of \mathbf{A} ; and $\mathbf{A}^{(m_1:m_2, n_1:n_2)}$ denotes a submatrix of \mathbf{A} defined by

$$\begin{bmatrix} \mathbf{A}^{(m_1, n_1)} & \mathbf{A}^{(m_1, n_1+1)} & \dots & \mathbf{A}^{(m_1, n_2)} \\ \mathbf{A}^{(m_1+1, n_1)} & \mathbf{A}^{(m_1+1, n_1+1)} & \dots & \mathbf{A}^{(m_1+1, n_2)} \\ \vdots & \vdots & \ddots & \vdots \\ \mathbf{A}^{(m_2, n_1)} & \mathbf{A}^{(m_2, n_1+1)} & \dots & \mathbf{A}^{(m_2, n_2)} \end{bmatrix}.$$

For any Hermitian matrix \mathbf{A} partitioned as $\begin{bmatrix} \mathbf{A}_{11} & \mathbf{A}_{12}^\dagger \\ \mathbf{A}_{12} & \mathbf{A}_{22} \end{bmatrix}$ with square submatrices \mathbf{A}_{11} and \mathbf{A}_{22} , $\mathbf{A}/\mathbf{A}_{22}$ denotes the generalized Schur complement of the block \mathbf{A}_{22} of \mathbf{A} , i.e., $\mathbf{A}_{11} - \mathbf{A}_{12}^\dagger \mathbf{A}_{22}^{-1} \mathbf{A}_{12}$, where \mathbf{A}_{22}^{-1} denotes the pseudo-inverse of \mathbf{A}_{22} . For two matrices \mathbf{A}_1 and \mathbf{A}_2 of appropriate sizes, $\mathbf{A}_1 \succeq \mathbf{A}_2$ and $\mathbf{A}_1 \succ \mathbf{A}_2$ denote that $\mathbf{A}_1 - \mathbf{A}_2 \in \mathcal{S}_+^n$ and $\mathbf{A}_1 - \mathbf{A}_2 \in \mathcal{S}_{++}^n$, respectively. We use $\mathcal{CN}(\mathbf{0}, \mathbf{Q})$ to denote the complex Gaussian distribution with zero mean and covariance \mathbf{Q} . Finally, we use \mathbf{I} to denote the identity matrix of an appropriate size, $\mathbf{0}$ to denote an all-zero matrix of an appropriate size, \mathbf{e}_m to denote the m -th column vector of \mathbf{I} , and \mathbf{E}_m to denote $\mathbf{e}_m \mathbf{e}_m^\dagger$.

II. SYSTEM MODEL AND PROBLEM FORMULATION

A. System Model

Consider the cooperative cellular network consisting of one CP and M single-antenna relay-like BSs (which will be called

relays for short later), which cooperatively serve K single-antenna users. In such network, the users and the relays are connected by noisy wireless channels, and the relays and the CP are connected by noiseless fronthaul links of finite capacities. Let $\mathcal{M} = \{1, 2, \dots, M\}$ and $\mathcal{K} = \{1, 2, \dots, K\}$ denote the sets of the relays and the users, respectively.

We first introduce the compression model from the CP to the relays. The beamformed signal at the CP is $\tilde{\mathbf{x}} = \sum_{k \in \mathcal{K}} \mathbf{v}_k s_k$, where $\mathbf{v}_k = [v_{k,1}, v_{k,2}, \dots, v_{k,M}]^\top$ is the $M \times 1$ beamforming vector and $s_k \sim \mathcal{CN}(0, 1)$ is the information signal for user k . Because of the limited capacities of the fronthaul links, the signal from the CP to the relays need to be first compressed before transmitted. Let the compression error be $\mathbf{e} = [e_1, e_2, \dots, e_m]^\top \sim \mathcal{CN}(\mathbf{0}, \mathbf{Q})$, where e_m denotes the error for compressing signals to relay m , and \mathbf{Q} is the covariance matrix of the compression noise. The transmitted signal of relay m is

$$x_m = \sum_{k \in \mathcal{K}} v_{k,m} s_k + e_m, \quad \forall m \in \mathcal{M}. \quad (1)$$

Then the received signal of user k is

$$y_k = \sum_{m \in \mathcal{M}} h_{k,m} x_m + z_k, \quad \forall k \in \mathcal{K},$$

where $h_{k,m}$ is the channel coefficient from relay m to user k , and $\{z_1, z_2, \dots, z_K\}$ are independent and identically distributed (i.i.d.) additive complex Gaussian noise distributed as $\mathcal{CN}(0, \sigma_k^2)$.

Under the above model, the received signal at user k is

$$y_k = \mathbf{h}_k^\dagger \left(\sum_{i \in \mathcal{K}} \mathbf{v}_i s_i \right) + \mathbf{h}_k^\dagger \mathbf{e} + z_k, \quad \forall k \in \mathcal{K},$$

where $\mathbf{h}_k = [h_{k,1}, h_{k,2}, \dots, h_{k,M}]^\dagger$ is the channel vector of user k . Then, the total transmit power of all the relays is

$$\sum_{k \in \mathcal{K}} \|\mathbf{v}_k\|^2 + \text{tr}(\mathbf{Q}).$$

The SINR of user k is

$$\gamma_k = \frac{|\mathbf{h}_k^\dagger \mathbf{v}_k|^2}{\sum_{j \neq k} |\mathbf{h}_k^\dagger \mathbf{v}_j|^2 + \mathbf{h}_k^\dagger \mathbf{Q} \mathbf{h}_k + \sigma_k^2}, \quad \forall k \in \mathcal{K}.$$

In order to fully utilize fronthaul links of finite capacities, we adopt the information-theoretically optimal multivariate compression strategy [26] to compress the signals from the CP to the relays. Without loss of generality, we assume that the compression order is from relay M to relay 1. Then the compression rate of relay m is given by

$$C_m = \log_2 \left(\frac{\sum_{k \in \mathcal{K}} |v_{k,m}|^2 + \mathbf{Q}^{(m,m)}}{\mathbf{Q}^{(m:M, m:M)} / \mathbf{Q}^{(m+1:M, m+1:M)}} \right), \quad \forall m \in \mathcal{M}.$$

B. Problem Formulation

Given a set of SINR targets for the users $\{\bar{\gamma}_k\}$ and a set of fronthaul capacities for the relays $\{\bar{C}_m\}$, we aim to minimize the total transmit power of all the users, as shown in (2):

$$\begin{aligned} \min_{\{\mathbf{v}_k\}, \mathbf{Q} \succeq \mathbf{0}} \quad & \sum_{k \in \mathcal{K}} \|\mathbf{v}_k\|^2 + \text{tr}(\mathbf{Q}) \\ \text{s.t.} \quad & \gamma_k \geq \bar{\gamma}_k, \quad \forall k \in \mathcal{K}, \\ & C_m \leq \bar{C}_m, \quad \forall m \in \mathcal{M}. \end{aligned} \quad (2)$$

Throughout the paper, we assume that the optimal covariance matrix \mathbf{Q} of problem (2) is positive definite. Otherwise, with a singular optimal \mathbf{Q} , $\mathbf{Q}^{(\bar{m}:M, \bar{m}:M)} / \mathbf{Q}^{(\bar{m}+1:M, \bar{m}+1:M)}$ will be zero for some \bar{m} , and hence $v_{k, \bar{m}}$ for all $k \in \mathcal{K}$ and $\mathbf{Q}^{(\bar{m}, \bar{m})}$ must be zero in order to satisfy the \bar{m} -th fronthaul rate constraint. In this case, $x_{\bar{m}}$ in (1) will be zero, which means that relay \bar{m} does not play any role in the whole transmission process, and we can instead consider a problem in the same form of (2) with a reduced set of relays excluding relay \bar{m} . In fact, this degenerate case rarely happens in practice.

Let $\mathbf{H}_k = \mathbf{h}_k \mathbf{h}_k^\dagger$ for all $k \in \mathcal{K}$ and $\bar{\eta}_m = 2^{\bar{C}_m} > 0$ for all $m \in \mathcal{M}$. By [41, Proposition 4], problem (2) is equivalent to the problem (P) at the top of the next page. The problem (P) with fixed beamformers, which is a semidefinite program (SDP), is studied in [41] to derive their uplink downlink duality results. Due to its SDP nature, the problem (P) with fixed beamformers naturally enjoys strong duality. However, the problem (P) itself is not in a convex form, and the existence of its convex reformulation is an unanswered question [41]. Notice that the convex reformulation technique proposed in [6], which turns the SINR constraints into a set of second order cone constraints via performing the square root operation on both sides of the SINR constraints, cannot be applied to the problem (P) because the additional variable \mathbf{Q} makes the resulting constraints non-convex.

In the following section, we will give a convex reformulation of the problem (P) by deriving the SDR of problem (P) and showing its tightness. Then, we will design an efficient algorithm for globally solving problem (P) by solving the enhanced KKT condition of its SDR.

III. SDR OF (P) AND ITS TIGHTNESS

Problem (P) is a quadratically constrained quadratic program. A well-known technique to tackle such problem is the SDR [42]. Applying the SDR technique to (P), we obtain

$$\begin{aligned} \min_{\{\mathbf{V}_k\}, \mathbf{Q} \succeq \mathbf{0}} \quad & \sum_{k \in \mathcal{K}} \text{tr}(\mathbf{V}_k) + \text{tr}(\mathbf{Q}) \\ \text{s.t.} \quad & a_k(\{\mathbf{V}_k\}, \mathbf{Q}) \geq 0, \quad \forall k \in \mathcal{K}, \\ & \mathbf{B}_m(\{\mathbf{V}_k\}, \mathbf{Q}) \succeq \mathbf{0}, \quad \forall m \in \mathcal{M}, \\ & \mathbf{V}_k \succeq \mathbf{0}, \quad \forall k \in \mathcal{K}, \end{aligned} \quad (3)$$

where

$$\begin{aligned} a_k(\{\mathbf{V}_k\}, \mathbf{Q}) &= - \left(\sum_{j \neq k} \text{tr}(\mathbf{V}_j \mathbf{H}_k) + \text{tr}(\mathbf{Q} \mathbf{H}_k) + \sigma_k^2 \right) \\ &\quad + \frac{1}{\bar{\gamma}_k} \text{tr}(\mathbf{V}_k \mathbf{H}_k), \\ \mathbf{B}_m(\{\mathbf{V}_k\}, \mathbf{Q}) &= \bar{\eta}_m \begin{bmatrix} \mathbf{0} & \mathbf{0} \\ \mathbf{0} & \mathbf{Q}^{(m:M, m:M)} \end{bmatrix} \\ &\quad - \mathbf{E}_m^\dagger \left(\sum_{k \in \mathcal{K}} \mathbf{v}_k \mathbf{v}_k^\dagger + \mathbf{Q} \right) \mathbf{E}_m. \end{aligned}$$

Since the problem (3) is convex, we consider its Lagrangian dual problem, which is given by

$$\begin{aligned} \max_{\beta \geq \mathbf{0}, \{\Lambda_m\}} \quad & \sum_{k \in \mathcal{K}} \beta_k \sigma_k^2 \\ \text{s.t.} \quad & \mathbf{I} + \mathbf{C}_k(\beta, \{\Lambda_m\}) - \frac{1}{\bar{\gamma}_k} \beta_k \mathbf{H}_k \succeq \mathbf{0}, \quad \forall k \in \mathcal{K}, \\ & \mathbf{D}(\beta, \{\Lambda_m\}) \succeq \mathbf{0}, \\ & \Lambda_m \succeq \mathbf{0}, \quad \forall m \in \mathcal{M}, \end{aligned} \quad (4)$$

where $\beta = [\beta_1, \beta_2, \dots, \beta_K]^\top$ with β_k being the dual variable associated with the k -th SINR constraint in problem (3), Λ_m is the dual variable associated with the m -th fronthaul rate constraint in problem (3), and

$$\begin{aligned} \mathbf{C}_k(\beta, \{\Lambda_m\}) &= \sum_{m \in \mathcal{M}} \mathbf{E}_m^\dagger \Lambda_m \mathbf{E}_m + \sum_{j \neq k} \beta_j \mathbf{H}_j, \\ \mathbf{D}(\beta, \{\Lambda_m\}) &= \mathbf{I} - \sum_{m \in \mathcal{M}} \bar{\eta}_m \begin{bmatrix} \mathbf{0} & \mathbf{0} \\ \mathbf{0} & \Lambda_m^{(m:M, m:M)} \end{bmatrix} \\ &\quad + \sum_{k \in \mathcal{K}} \beta_k \mathbf{H}_k + \sum_{m \in \mathcal{M}} \mathbf{E}_m^\dagger \Lambda_m \mathbf{E}_m. \end{aligned}$$

An important line of research on the SDR is to study its tightness [42]–[44]. In the following theorem, we show that the SDR in (3) is tight (if it is feasible), i.e., it always has a rank-one solution. This reveals the hidden convexity in the seemingly non-convex problem (P) and shows that the problem admits a convex reformulation, which answers a question in [41, Section IX-B].

Theorem 1: Suppose that problem (3) is (strongly) feasible, and let $(\{\mathbf{V}_k\}, \mathbf{Q})$ be its solution. Then \mathbf{V}_k is of rank one for all $k \in \mathcal{K}$.

Proof: Since $(\{\mathbf{V}_k\}, \mathbf{Q})$ is a solution of problem (3), there must exist dual multipliers β and $\{\Lambda_m\}$ such that the Karush-Kuhn-Tucker (KKT) conditions of problem (3) hold. In particular, the complementary slackness conditions

$$\text{tr} \left(\mathbf{V}_k \left(\mathbf{I} + \mathbf{C}_k(\beta, \{\Lambda_m\}) - \frac{1}{\bar{\gamma}_k} \beta_k \mathbf{H}_k \right) \right) = 0, \quad \forall k \in \mathcal{K}$$

hold. Since $\mathbf{I} + \mathbf{C}_k(\beta, \{\Lambda_m\})$ is positive definite and \mathbf{H}_k is rank-one and positive semidefinite, it follows that

$$\text{rank} \left(\mathbf{I} + \mathbf{C}_k(\beta, \{\Lambda_m\}) - \frac{1}{\bar{\gamma}_k} \beta_k \mathbf{H}_k \right) \geq M - 1, \quad \forall k \in \mathcal{K},$$

which, together with the complementary slackness condition and the rank inequality, implies that $\text{rank}(\mathbf{V}_k) \leq 1$ for all $k \in \mathcal{K}$. If $\mathbf{V}_k = \mathbf{0}$, i.e., user k is assigned with a zero beamformer, then its corresponding SINR constraint will be violated. Therefore, all optimal \mathbf{V}_k are rank-one. The proof is complete. \square

Two remarks on Theorem 1 are as follows. First, Theorem 1 offers a way of globally solving problem (P) via solving its SDR (3), which provides an important benchmark for performance evaluation of other algorithms for solving problem (P). Second, it is well known that the KKT conditions are sufficient and necessary for the global solution of problem (3). It will become more clear that the KKT conditions play a central role in solving problem (3). In the following, we shall design an efficient fixed point algorithm for solving the KKT conditions of problem (3).

$$\begin{aligned}
& \min_{\{\mathbf{v}_k\}, \mathbf{Q} \succeq \mathbf{0}} \sum_{k \in \mathcal{K}} \|\mathbf{v}_k\|^2 + \text{tr}(\mathbf{Q}) \\
& \text{s.t.} \quad \frac{1}{\tilde{\gamma}_k} \mathbf{v}_k^\dagger \mathbf{H}_k \mathbf{v}_k - \left(\sum_{j \neq k} \mathbf{v}_j^\dagger \mathbf{H}_k \mathbf{v}_j + \text{tr}(\mathbf{Q} \mathbf{H}_k) + \sigma_k^2 \right) \geq 0, \quad \forall k \in \mathcal{K}, \\
& \quad \bar{\eta}_m \begin{bmatrix} \mathbf{0} & \mathbf{0} \\ \mathbf{0} & \mathbf{Q}^{(m:M, m:M)} \end{bmatrix} - \mathbf{E}_m^\dagger \left(\sum_{k \in \mathcal{K}} \mathbf{v}_k \mathbf{v}_k^\dagger + \mathbf{Q} \right) \mathbf{E}_m \succeq \mathbf{0}, \quad \forall m \in \mathcal{M}.
\end{aligned} \tag{P}$$

IV. PROPOSED FIXED POINT ITERATION ALGORITHM

In this section, we first combine the special structures of the solution of the problem (3) with its KKT conditions to derive a new set of conditions, which is referred to as the enhanced KKT conditions. Then, we present an efficient way of solving the enhanced KKT conditions via two fixed point iterations and thus an efficient algorithm for solving the problem (3).

First, recall that the KKT conditions of an SDP consists of the dual feasibility conditions, the primal feasibility conditions, and the complementary slackness conditions. Specifically, supposing $\{\mathbf{V}_k\}$ and \mathbf{Q} are the primal solutions, and β and $\{\Lambda_m\}$ are the dual solutions, the complementary conditions of problem (3) are given by

$$\text{tr}(\mathbf{Q} \mathbf{D}(\beta, \{\Lambda_m\})) = 0, \tag{5}$$

$$\text{tr} \left(\mathbf{V}_k \left(\mathbf{I} + \mathbf{C}_k(\beta, \{\Lambda_m\}) - \frac{1}{\tilde{\gamma}_k} \beta_k \mathbf{H}_k \right) \right) = 0, \quad \forall k \in \mathcal{K}, \tag{6}$$

and

$$\text{tr}(\Lambda_m \mathbf{B}_m(\{\mathbf{V}_k\}, \mathbf{Q})) = 0, \quad \forall m \in \mathcal{M}. \tag{7}$$

Now, we combine the KKT conditions with the specific structures of the problem (3) to derive the enhanced KKT conditions. Specifically, the dual feasibility conditions are enhanced into the following conditions:

$$\mathbf{D}(\beta, \{\Lambda_m\}) = \mathbf{0}, \tag{8}$$

$$\left. \begin{aligned} & \text{rank}(\Lambda_m) \leq 1, \quad \Lambda_m \succeq \mathbf{0}, \quad \forall m \in \mathcal{M}, \\ & \Lambda_m^{(1:m-1, 1:m)} = \mathbf{0}, \quad \Lambda_m^{(m:M, 1:m-1)} = \mathbf{0}, \quad \forall m \in \mathcal{M}, \end{aligned} \right\} \tag{9}$$

$$\beta \geq \mathbf{0}, \tag{10}$$

$$\left. \begin{aligned} & \text{rank} \left(\mathbf{I} + \mathbf{C}_k(\beta, \{\Lambda_m\}) - \frac{1}{\tilde{\gamma}_k} \beta_k \mathbf{H}_k \right) \\ & \quad = M - 1, \quad \forall m \in \mathcal{M}, \\ & \mathbf{I} + \mathbf{C}_k(\beta, \{\Lambda_m\}) - \beta_k \mathbf{H}_k \succeq \mathbf{0}, \quad \forall m \in \mathcal{M}, \end{aligned} \right\} \tag{11}$$

where (8) is a result of replacing the inequality in the dual feasibility condition $\mathbf{D}(\beta, \{\Lambda_m\}) \succeq \mathbf{0}$ with equality, which is justified by the complementary slackness condition (5) and $\mathbf{Q} \succ \mathbf{0}$; (9) is shown in Appendix A; and (11) has already been shown in the proof of Theorem 1. Furthermore, the primal feasibility conditions are enhanced into the following conditions:

$$\left\{ \begin{aligned} & \mathbf{V}_k \succeq \mathbf{0}, \quad \text{rank}(\mathbf{V}_k) = 1, \quad \forall k \in \mathcal{K}, \\ & a_k(\{\mathbf{V}_k\}, \mathbf{Q}) = 0, \quad \forall k \in \mathcal{K}, \\ & \mathbf{B}_m(\{\mathbf{V}_k\}, \mathbf{Q}) \succeq \mathbf{0}, \quad \forall m \in \mathcal{M}, \\ & \mathbf{Q} \succeq \mathbf{0}, \end{aligned} \right. \tag{12}$$

$$\tag{13}$$

$$\tag{14}$$

$$\tag{15}$$

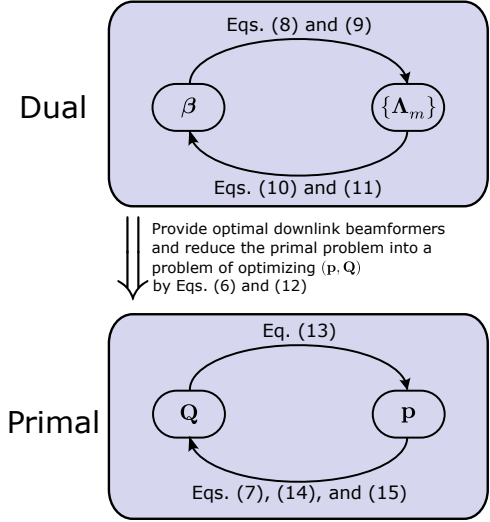


Fig. 1. The flow chart of the proposed algorithm for solving the enhanced KKT conditions.

where (12) is shown by Theorem 1, and (13) is shown in Appendix A. The enhanced KKT conditions, i.e., Eqs. (6)–(15), defines a subset of KKT points. The important thing here is that this subset is not empty and contains a solution to the problem (3).

Next, we shall design an algorithm for solving the enhanced KKT conditions. The basic idea is to first solve the enhanced dual feasibility conditions, i.e., Eqs. (8)–(11), for the dual variables β and $\{\Lambda_m\}$; and then plug them into the rest of the enhanced KKT conditions to solve for the primal variables $\{\mathbf{V}_k\}$ and \mathbf{Q} . The flow chart of the proposed algorithm for solving the enhanced KKT conditions is illustrated in Fig. 1.

A. Solving for the Dual Variables

1) *Solving Eqs. (8) and (9) for $\{\Lambda_m\}$* : Suppose that β is given, we first find $\{\Lambda_m\}$ that satisfy Eqs. (8) and (9). Define

$$\Gamma(\beta) = \mathbf{I} + \sum_{k \in \mathcal{K}} \beta_k \mathbf{H}_k. \tag{16}$$

Then Eq. (8) is equivalent to

$$\sum_{m=1}^M \eta_m \begin{bmatrix} \mathbf{0} & \mathbf{0} \\ \mathbf{0} & \Lambda_m^{(m:M, m:M)} \end{bmatrix} - \sum_{m=1}^M \mathbf{E}_m^\dagger \Lambda_m \mathbf{E}_m = \Gamma(\beta). \tag{17}$$

We know from the special properties of $\{\Lambda_m\}$ in Eq. (9) that only Λ_1 affects the first row and column of matrix $\Gamma(\beta)$. Therefore, the entries in the first row of Λ_1 should be

$$\left[\frac{1}{\eta_1-1} \Gamma(\beta)^{(1,1)}, \frac{1}{\eta_1} \Gamma(\beta)^{(1,2:M)} \right].$$

Since Λ_1 is of rank one, we can further obtain all entries of Λ_1 based on its entries in the first row, which is

$$\Lambda_1 = \begin{bmatrix} \frac{1}{\eta_1-1} \Gamma(\beta)^{(1,1)} & \frac{1}{\eta_1} \Gamma(\beta)^{(1,2:M)} \\ \frac{1}{\eta_1} \Gamma(\beta)^{(2:M,1)} & \frac{\eta_1-1}{\eta_1^2} \frac{\Gamma(\beta)^{(2:M,1)} \Gamma(\beta)^{(1,2:M)}}{\Gamma(\beta)^{(1,1)}} \end{bmatrix}. \quad (18)$$

After Λ_1 is obtained, we can subtract all terms related to Λ_1 from both sides of (17) and denote the known right-hand side as $\Gamma_2(\beta)$. Then, after the subtraction, (17) becomes

$$\sum_{m=2}^M \eta_m \begin{bmatrix} \mathbf{0} & \mathbf{0} \\ \mathbf{0} & \Lambda_m^{(m:M,m:M)} \end{bmatrix} - \sum_{m=2}^M \mathbf{E}_m^\dagger \Lambda_m \mathbf{E}_m = \Gamma_2(\beta). \quad (19)$$

For general $2 \leq m \leq M$, denote the right-hand side of (17) after $\Lambda_1, \Lambda_2, \dots, \Lambda_{m-1}$ are solved and subtracted from both sides as $\Gamma_m(\beta)$. By comparing the m -th row of the obtained equation and using the rank-one property of Λ_m , we can obtain Λ_m , whose non-zero part $\Lambda_m^{(m:M,m:M)}$ is

$$\begin{bmatrix} \frac{1}{\bar{\eta}_m-1} \Gamma_m(\beta)^{(m,m)} & \frac{1}{\bar{\eta}_m} \Gamma_m(\beta)^{(m,m+1:M)} \\ \frac{1}{\bar{\eta}_m} \Gamma_m(\beta)^{(m+1:M,m)} & \frac{\bar{\eta}_m-1}{\bar{\eta}_m^2} \frac{\Gamma_m(\beta)^{(m+1:M,m)} \Gamma_m(\beta)^{(m,m+1:M)}}{\Gamma_m(\beta)^{(m,m)}} \end{bmatrix}. \quad (20)$$

We can repeat the above procedure until all $\{\Lambda_m\}$ are obtained. These solutions, depending on the given β , are denoted as $\{\Lambda_m(\beta)\}$. Please refer to Appendix C in the Supplementary Material for the details of the above procedure.

2) *Solving Eqs. (10) and (11) for β* : Now suppose that $\{\Lambda_m\}$ are given, we would like to find β that satisfies Eqs. (10) and (11). Since $\mathbf{I} + \mathbf{C}_k(\beta, \{\Lambda_m\}) \succ \mathbf{0}$ and $\mathbf{H}_k \succeq \mathbf{0}$ is rank-one, there exists a unique β_k such that one and only one eigenvalue of $\mathbf{I} + \mathbf{C}_k(\beta, \{\Lambda_m\}) - \frac{1}{\bar{\gamma}_k} \beta_k \mathbf{H}_k$ is equal to zero. Such β_k admits the following closed-form solution:

$$\beta_k(\{\Lambda_m\}, \beta) = \frac{\bar{\gamma}_k}{\mathbf{h}_k^\dagger (\mathbf{I} + \mathbf{C}_k(\beta, \{\Lambda_m\}))^{-1} \mathbf{h}_k}, \quad \forall k \in \mathcal{K}. \quad (21)$$

3) *Dual fixed point iteration*: From the above discussion, we know that if β is known, one can get $\{\Lambda_m(\beta)\}$ such that Eqs. (8) and (9) hold. Plug this solution $\{\Lambda_m(\beta)\}$ into (21). Then, if one can find β that satisfy

$$\beta_k = I_k(\beta) \triangleq \beta_k(\{\Lambda_m(\beta)\}, \beta), \quad \forall k \in \mathcal{K}, \quad (22)$$

all Eqs. (8)–(11) are satisfied. If we define $I(\beta) = [I_1(\beta), I_2(\beta), \dots, I_K(\beta)]^\top$, then solving (22) is to find the fixed point of the function $I(\cdot)$, namely solving

$$\beta = I(\beta). \quad (23)$$

It is worth highlighting that the computational cost of evaluating the function $I(\cdot)$ in (23) is quite cheap. The dominant computation is to compute $\mathbf{C}_k^{-1} \mathbf{h}_k$ for $k \in \mathcal{K}$, where \mathbf{C}_k is an $M \times M$ positive definite matrix, and the arithmetic complexity is $\mathcal{O}(KM^3)$. Furthermore, as will be shown later

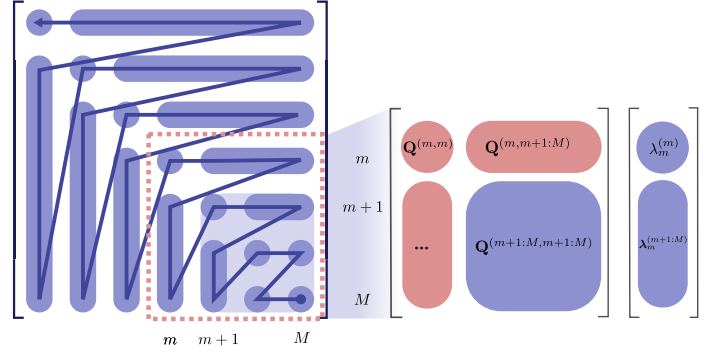


Fig. 2. An illustration of solving (26) for \mathbf{Q} .

in Theorem 2, Eq. (23) can be easily solved via the dual fixed point iteration

$$\beta^{(i+1)} = I(\beta^{(i)}) \quad (24)$$

with a linear convergence rate. This fact, together with the cheap evaluation of the function $I(\cdot)$ at each iteration, shows that the above fixed point iteration in (24) provides an efficient way of solving the enhanced dual feasibility conditions, i.e., Eqs. (8)–(11).

B. Solving for the Primal Variables

Suppose that we already have β and $\{\Lambda_m\}$ that satisfy the enhanced dual feasibility conditions. We still need to find $\{\mathbf{V}_k\}$ and \mathbf{Q} that satisfy the rest of the enhanced KKT conditions. By Eq. (12), let $\mathbf{V}_k = p_k \mathbf{v}_k \mathbf{v}_k^\dagger$ with $\|\mathbf{v}_k\| = 1$. Then Eq. (6) becomes $\mathbf{v}_k^\dagger (\mathbf{C}_k - \beta_k \mathbf{H}_k) \mathbf{v}_k = 0$. Combining this with Eq. (11) gives

$$(\mathbf{C}_k - \beta_k \mathbf{H}_k) \mathbf{v}_k = \mathbf{C}_k \mathbf{v}_k - \beta_k \mathbf{h}_k (\mathbf{h}_k^\dagger \mathbf{v}_k) = \mathbf{0}.$$

Hence, \mathbf{v}_k can be solved explicitly as follows:

$$\mathbf{v}_k = \frac{\mathbf{C}_k^{-1} \mathbf{h}_k}{\|\mathbf{C}_k^{-1} \mathbf{h}_k\|}.$$

Define $\mathbf{p} = [p_1, p_2, \dots, p_K]^\top$. We still need to find \mathbf{Q} and \mathbf{p} such that Eqs. (7) and (13)–(15) hold.

1) *Solving Eq. (13) for \mathbf{p}* : Substituting $\hat{\mathbf{V}}_k = \mathbf{v}_k \mathbf{v}_k^\dagger$ into (13), one has

$$\frac{1}{\bar{\gamma}_k} p_k \text{tr}(\hat{\mathbf{V}}_k \mathbf{H}_k) - \left(\sum_{j \neq k} p_j \text{tr}(\hat{\mathbf{V}}_j \mathbf{H}_k) + \text{tr}(\mathbf{Q} \mathbf{H}_k) + \sigma_k^2 \right) = 0.$$

Then one can solve for p_k as follows:

$$p_k(\mathbf{Q}, \mathbf{p}) = \frac{\bar{\gamma}_k \left(\sum_{j \neq k} p_j \text{tr}(\hat{\mathbf{V}}_j \mathbf{H}_k) + \text{tr}(\mathbf{Q} \mathbf{H}_k) + \sigma_k^2 \right)}{\text{tr}(\hat{\mathbf{V}}_k \mathbf{H}_k)}. \quad (25)$$

2) *Solving Eqs. (7), (14), and (15) for \mathbf{Q}* : Next, given \mathbf{p} , we shall obtain \mathbf{Q} such that Eqs. (7), (14), and (15) hold. By Eq. (9), one can decompose Λ_m into $\Lambda_m = \lambda_m \lambda_m^\dagger$, where $\lambda_m = [\mathbf{0}, \lambda_m^{(m)}, \lambda_m^{(m+1)}, \dots, \lambda_m^{(M)}]^\top$. This decomposition, together with Eqs. (14) and (7), implies

$$\mathbf{B}_m \left(\left\{ p_k \hat{\mathbf{V}}_k \right\}, \mathbf{Q} \right) \lambda_m = \mathbf{0}, \quad \forall m \in \mathcal{M}. \quad (26)$$

We shall solve (26) from $m = M$ to $m = 1$ and obtain the desired \mathbf{Q} in the order shown in the left-hand side of Fig. 2. More specifically, when $m = M$, it follows that

$$\mathbf{Q}^{(M,M)} = \frac{\sum_{k \in \mathcal{K}} p_k \hat{\mathbf{V}}_k^{(M,M)}}{\bar{\eta}_m - 1}. \quad (27)$$

When $m < M$, we can substitute the known $\mathbf{Q}^{(m+1:M, m+1:M)}$ into the m -th equation in Eq. (26), which gives a linear equation with variables $\mathbf{Q}^{(m,m)}$, $\mathbf{Q}^{(m, m+1:M)}$, and $\mathbf{Q}^{(m+1:M, m)}$. This linear equation is illustrated in the right-hand side of Fig. 2, where the known variables are marked in blue and the unknown variables are marked in red. We first solve $\mathbf{Q}^{(m+1:M, m)}$ by using the last $M - m + 1$ equations in the right-hand side of Fig. 2. The solution is given by

$$\mathbf{Q}^{(m+1:M, m)} = -\frac{\mathbf{Q}^{(m+1:M, m+1:M)} \boldsymbol{\lambda}_m^{(m+1:M)}}{\boldsymbol{\lambda}_m^{(m)}}. \quad (28)$$

Then, by Eq. (15), $\mathbf{Q}^{(m, m+1:M)}$ is given by the Hermitian transpose of $\mathbf{Q}^{(m+1:M, m)}$. Finally, we can further obtain $\mathbf{Q}^{(m,m)}$ by using the first equation in the right-hand side of Fig. 2, which is given by

$$\mathbf{Q}^{(m,m)} = \frac{\bar{\eta}_m \boldsymbol{\lambda}_m^{(m+1:M)\dagger} \mathbf{Q}^{(m+1:M, m+1:M)} \boldsymbol{\lambda}_m^{(m+1:M)}}{\bar{\eta}_m - 1} + \frac{1}{\bar{\eta}_m - 1} \sum_{k \in \mathcal{K}} p_k \hat{\mathbf{V}}_k^{(m,m)}. \quad (29)$$

Using the above tricks, we can obtain the solution \mathbf{Q} of Eq. (26). We denote the solution as $\mathbf{Q}(\mathbf{p})$, because the solution depends on the given \mathbf{p} .

3) *Primal fixed point iteration*: Based on the above discussion, we know that if \mathbf{p} is known, one can get $\mathbf{Q}(\mathbf{p})$ such that Eqs. (7), (14), and (15) hold. Plugging this solution into (25) gives

$$p_k = J_k(\mathbf{p}) \triangleq p_k(\mathbf{Q}(\mathbf{p}), \mathbf{p}), \quad \forall k \in \mathcal{K}. \quad (30)$$

Define $J(\mathbf{p}) = [J_1(\mathbf{p}), J_2(\mathbf{p}), \dots, J_K(\mathbf{p})]^\top$. Then Eq. (30) becomes the problem of finding the fixed point of the function $J(\cdot)$, i.e.,

$$\mathbf{p} = J(\mathbf{p}). \quad (31)$$

If one can find \mathbf{p} such that (31) holds, then \mathbf{p} and $\mathbf{Q}(\mathbf{p})$ will satisfy Eqs. (7) and (13)–(15), and further $\{p_k \hat{\mathbf{V}}_k\}$ and $\mathbf{Q}(\mathbf{p})$ will solve the enhanced KKT conditions.

We shall show in Theorem 2 that Eq. (31) can be efficiently solved via the fixed point iteration

$$\mathbf{p}^{(i+1)} = J(\mathbf{p}^{(i)}), \quad (32)$$

and the convergence rate of the fixed point iteration is linear. Moreover, each evaluation of $J(\cdot)$ is computationally cheap. More specifically, the computation mainly consists of two parts: first, the total complexity of the procedure described by (27)–(29) is $\mathcal{O}(M^3)$; second, after $\text{tr}(\hat{\mathbf{V}}_j \mathbf{H}_k)$ for all j and k are computed, the complexity of computing $p_k(\mathbf{Q}, \mathbf{p})$ in (25) is $\mathcal{O}(KM^2)$. As a result, the total complexity of each evaluation of $J(\cdot)$ is $\mathcal{O}((K+M)M^2)$. Due to the low per-iteration complexity and the linear convergence rate, the above fixed point iteration in (32) provides an efficient way of solving the enhanced KKT conditions after solving the dual problem.

C. Proposed Fixed Point Iteration (FPI) Algorithm

Now, we present the algorithm for solving problem (3) (which is equivalent to problem (P)). The algorithm first finds $\boldsymbol{\beta}$ and $\{\boldsymbol{\Lambda}_m\}$ that satisfy the enhanced dual feasibility conditions; with found $\boldsymbol{\beta}$ and $\{\boldsymbol{\Lambda}_m\}$ fixed, the algorithm then finds $\{\mathbf{V}_k\}$ and \mathbf{Q} that satisfy the rest of the enhanced KKT conditions. Hence, $\{\mathbf{V}_k\}$, \mathbf{Q} , $\boldsymbol{\beta}$, and $\{\boldsymbol{\Lambda}_m\}$ together satisfy the enhanced KKT conditions and thus is a KKT point of problem (3). Since $\text{rank}(\mathbf{V}_k) = 1$ for all k , we can recover the optimal solution for problem (P). The pseudocodes of the proposed FPI algorithm are given in Algorithm 1.

Algorithm 1 Proposed FPI Algorithm for Solving Problem (P)

- 1: Find $\boldsymbol{\beta}$ and $\{\boldsymbol{\Lambda}_m\}$ that satisfy the enhanced dual feasibility conditions by performing the fixed point iteration in (23) on $\boldsymbol{\beta}$ until the desired error bound is met.
 - 2: Find $\{\mathbf{V}_k\}$ and \mathbf{Q} that satisfy the rest of the enhanced KKT conditions by performing the fixed point iteration in (31) on \mathbf{p} until the desired error bound is met.
 - 3: Find \mathbf{v}_k such that $\mathbf{V}_k = \mathbf{v}_k \mathbf{v}_k^\dagger$, $\forall k \in \mathcal{K}$.
 - 4: **Output**: $\{\mathbf{v}_k\}$ and \mathbf{Q} .
-

D. Theoretical Guarantees

1) *Convergence and convergence rate of FPI*: We have the following convergence and convergence rate guarantee of the proposed FPI algorithm.

Theorem 2: If problem (3) is (strongly) feasible, both the dual fixed point iteration (24) and the primal fixed point iteration (32) in the proposed FPI algorithm converge linearly.

Proof: See Appendix B. \square

The following convergence rate results have been shown for the dual/primal fixed point iteration in Appendix B. Let $\boldsymbol{\gamma} = [\gamma_1, \gamma_2, \dots, \gamma_K]^\top$. Define the metric $\mu: \mathbb{R}_{++}^K \times \mathbb{R}_{++}^K \rightarrow \mathbb{R}_+^K$ as

$$\mu(\boldsymbol{\beta}, \boldsymbol{\gamma}) = \max_{k \in \mathcal{K}} \left| \log_e \left(\frac{\beta_k}{\gamma_k} \right) \right|, \quad (33)$$

which is proposed in [45]. Under this metric, the asymptotic linear convergence rate of the dual fixed point iteration (24) is given by

$$\limsup_{i \rightarrow \infty} \frac{\mu(\boldsymbol{\beta}^{(i+1)}, \boldsymbol{\beta}^*)}{\mu(\boldsymbol{\beta}^{(i)}, \boldsymbol{\beta}^*)} \leq \frac{\lambda(\boldsymbol{\beta}^*)}{1 + \lambda(\boldsymbol{\beta}^*)}, \quad (34)$$

where $\boldsymbol{\beta}^*$ is the fixed point of $I(\cdot)$ and

$$\lambda(\boldsymbol{\beta}) = \max_{k \in \mathcal{K}} \{\|\mathbf{C}_k(\boldsymbol{\beta}, \{\boldsymbol{\Lambda}_m(\boldsymbol{\beta})\})\|_2\}. \quad (35)$$

Besides, the linear convergence rate of the primal fixed point iteration (32) is governed by the spectral radius of \mathbf{G} in $J(\cdot)$, where the entries of \mathbf{G} are given by

$$G_{kj} = \begin{cases} \frac{\bar{\gamma}_k (\text{tr}(\mathbf{Q}(\mathbf{e}_k) \mathbf{H}_k))}{\text{tr}(\hat{\mathbf{V}}_k \mathbf{H}_k)}, & \text{if } j = k, \\ \frac{\bar{\gamma}_k (\text{tr}(\hat{\mathbf{V}}_j \mathbf{H}_k) + \text{tr}(\mathbf{Q}(\mathbf{e}_k) \mathbf{H}_k))}{\text{tr}(\hat{\mathbf{V}}_k \mathbf{H}_k)}, & \text{otherwise.} \end{cases} \quad (36)$$

The above convergence rate results shed useful insights into the convergence behavior of the proposed FPI algorithm, and in particular the efficiency of the proposed FPI algorithm is determined by the given problem instance. In general, the proposed FPI algorithm will converge slower when the considered problem approaches the singular boundary¹. To be specific, as we increase the SINR targets $\{\bar{\gamma}_k\}$ in problem (3) (with all the other parameters being unchanged), the corresponding problem will approach the singular boundary. In the dual fixed point iteration (24), as $\{\bar{\gamma}_k\}$ increases, β^* , which depends on $\{\bar{\gamma}_k\}$, will increase. Combining this with the fact that $\lambda(\beta)$ in (35) is an increasing function of β , we have that $\lambda(\beta^*)$ will increase, and hence the right-hand side of (34) will increase as well. This clearly shows that the convergence rate of the dual fixed point iteration (24) will become slower as the problem approaches the singular boundary. The same happens for the primal fixed point iteration (32). When the SINR targets $\{\bar{\gamma}_k\}$ in problem (3) increase, the spectral radius of \mathbf{G} in (36) increases, and the convergence rate of the primal fixed point iteration (31) becomes slower. This shows that the primal fixed point iteration (32) will become slower as the problem approaches the singular boundary.

2) Global optimality of FPI and infeasibility detection:

First, we have the following global optimality guarantee of the proposed FPI algorithm.

Theorem 3: If problem (3) is (strongly) feasible, then the FPI algorithm returns the optimal solution of problem (P).

Proof: Let \mathbf{p} be the converged solution of the primal fixed point iteration (32), and β be the converged solution of the dual fixed point iteration (24) in the FPI algorithm. First, for given \mathbf{p} , $\mathbf{Q}(\mathbf{p})$ in the FPI algorithm is obtained such that Eqs. (14)–(15) hold; for given β , $\{\Lambda_m(\beta)\}$ in the FPI algorithm are obtained such that Eqs. (8) and (9) hold. Second, $\{\hat{\mathbf{V}}_k\}$ are solved such that Eqs. (6) and (12) hold. Furthermore, the convergence of β and \mathbf{p} shows that Eqs. (11), (10), and (13) hold. In all, the primal variables $\{p_k \hat{\mathbf{V}}_k\}$ and $\mathbf{Q}(\mathbf{p})$, together with the dual variables β and $\{\Lambda_m(\beta)\}$, satisfy all conditions (8)–(15) in the enhanced KKT system, and hence is a global solution of problem (3) (which is equivalent to (P)). \square

In Theorem 3, we assume that problem (3) is feasible. A natural question is how the FPI algorithm behaves when problem (3) is infeasible. According to the weak duality, any dual feasible solution provides a lower bound on the optimal value of problem (3). By the monotonicity of $I(\cdot)$ shown in Appendix B, if we initialize the dual fixed point iteration (24) with $\beta^{(0)}$ satisfying $\beta^{(0)} \leq I(\beta^{(0)})$ and $\beta^{(0)} \neq I(\beta^{(0)})$, e.g., $\beta^{(0)} = \mathbf{0}$, we have

$$I(\beta^{(i)}) = \beta^{(i+1)} \geq \beta^{(i)} \text{ and } \beta^{(i+1)} \neq \beta^{(i)}, \text{ for all } i.$$

This shows that $(\beta^{(i)}, \{\Lambda_m(\beta^{(i)})\})$ is a dual feasible solution, and hence the corresponding strictly increasing dual objective value serves as a lower bound on the optimal value of problem (3). If we observe that this dual objective value is greater than a preset upper bound in practice (e.g., the system power

¹The singular boundary here means the boundary of the achievable SINR region by problem (3) with given channel conditions and compression capacities.

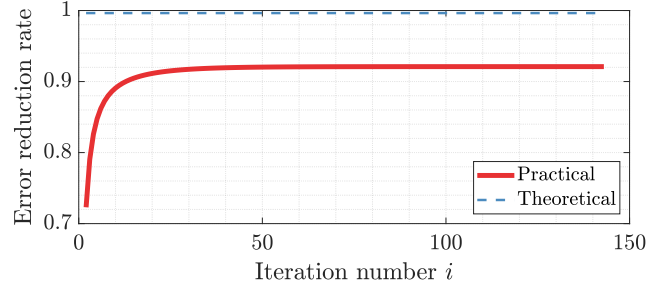


Fig. 3. The convergence rate of the dual fixed point iteration (24) with $\gamma = 0.07$.

limit), then we claim that problem (3) is infeasible. In this sense, our proposed FPI algorithm can automatically detect the infeasibility of problem (3) when the problem is infeasible.

In summary, two key features of our proposed FPI algorithm are as follows: (1) it is guaranteed to find the global solution of problem (3) when the problem is feasible and is able to detect its infeasibility when the problem is infeasible (with an appropriate initialization); (2) it enjoys a linear convergence rate, and it converges faster when the problem instance is far away from the singular boundary (compared with the problem instance close to the singular boundary).

V. NUMERICAL RESULTS

In this section, the performance of the proposed FPI algorithm is evaluated and compared with existing SOTA algorithms. The default scenario that we consider is a cooperative network with $M = 8$ single-antenna relays serving $K = 10$ single-antenna users. The channel between the relays and users is generated by i.i.d complex Gaussian distribution with zero mean and unit variance. In the following numerical experiments, the users' SINR targets are considered identical, i.e., $\gamma = \bar{\gamma}_1 = \bar{\gamma}_2 = \dots = \bar{\gamma}_K$, and all the relays' fronthaul capacities are set to $\log_2(1.1)$. Furthermore, we initialize the dual fixed point iteration (24) and the primal fixed point iteration (32) with zero power vectors in the proposed FPI algorithm.

A. Behaviors of Proposed FPI Algorithm

In this subsection, we first study the practical behaviors of the proposed FPI algorithm. We are interested in the convergence rate of the proposed FPI algorithm and how it behaves when the corresponding problem instances are close to the singular boundary.

Fig. 3 and Fig. 4 show the linear convergence rate of the proposed FPI algorithm. In particular, Fig. 3 shows the linear convergence rate of the dual fixed point iteration (24). In Fig. 3, the error reduction rate $\frac{\mu(\beta^{(i+1)}, \beta^*)}{\mu(\beta^{(i)}, \beta^*)}$ is plotted against the iteration number i and compared with the theoretical upper bound $\frac{\lambda(\beta^*)}{1 + \lambda(\beta^*)}$ given in (34) for a given SINR target $\gamma = 0.07$. We can observe from the figure that the convergence rate of the dual fixed point iteration (24) is indeed linear, albeit the upper bound in (34) is conservative and does not match the practical

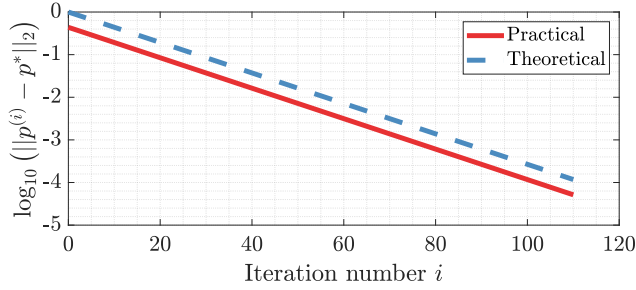


Fig. 4. The convergence rate of the primal fixed point iteration (32).

TABLE I
THEORETICAL AND PRACTICAL CONVERGENCE RATE COMPARISON FOR
DIFFERENT SINR TARGETS γ

SINR target γ	0.01	0.03	0.05	0.07	0.075
Theoretical	0.9278	0.9585	0.9809	0.9964	0.9994
Practical	0.1440	0.4122	0.6668	0.9210	0.9861

convergence rate. Fig. 4 verifies the linear convergence rate of the primal fixed point iteration, and the theoretical and practical convergence rates are well-matched.

Table. I shows the practical asymptotic linear convergence rate and the theoretical upper bound $\frac{\lambda(\beta^*)}{1+\lambda(\beta^*)}$ given in (34) for different SINR targets γ . As is shown in the table, when the SINR target γ increases (i.e. the feasible problem approaches the singular boundary), the theoretical and practical asymptotic convergence rates become close to each other, and both of them increase to one. This verifies the convergence behavior analysis below (36) and shows that the theoretical upper bound $\frac{\lambda(\beta^*)}{1+\lambda(\beta^*)}$ is useful in characterizing the (intrinsic) difficulty of the problem.

Now we look at the behaviors of the proposed FPI algorithm when the problem instances are close to the singular boundary. Fig. 5 shows the behavior of the FPI algorithm in both feasible and infeasible cases. In both Figs. 5 (a) and 5 (b), three problem instances with different SINR targets γ are plotted. Figs. 5 (a) plots the dual/primal objective values versus the iteration number when the problems are feasible. The optimal values of the three problem instances are plotted in the gray dotted line, respectively in Fig. 5 (a). As expected (and observed from Fig. 5 (a)), both the dual and primal objective values monotonically increase and finally converge to the optimal value. Fig. 5 (b) plots the dual objective values versus the iteration number when the problems are infeasible. In this case, as analyzed below Theorem 3 and observed in Fig. 5 (b), the dual objective values monotonically increase to infinity. It can be seen clearly from Fig. 5 that the proposed FPI algorithm converges/diverges slower when the problem instances are close to the singular boundary in both feasible and infeasible cases.

In the following numerical experiments, the problems considered are feasible and relatively far from the singular boundary.

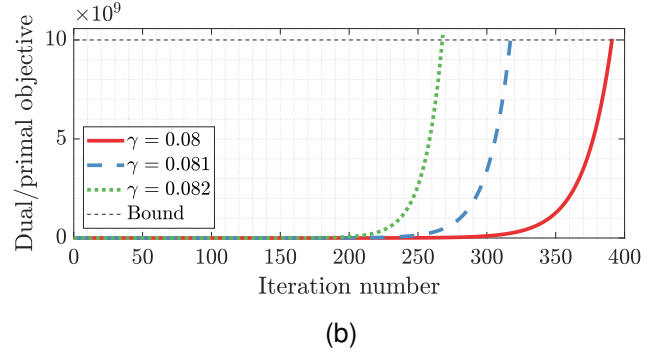
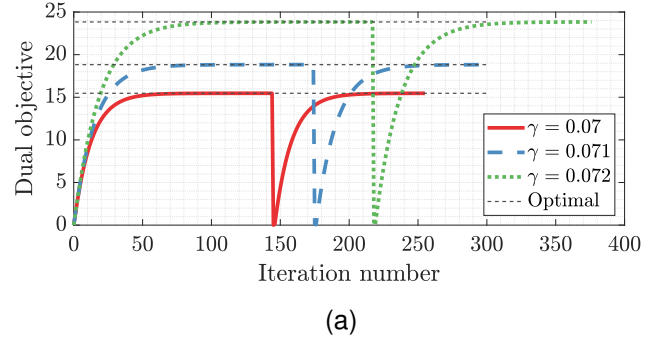


Fig. 5. (a) The dual/primal objective values versus the iteration number for feasible problem instances with different SINR targets γ ; (b) The dual objective values versus the iteration number for infeasible problem instances with different SINR targets γ .

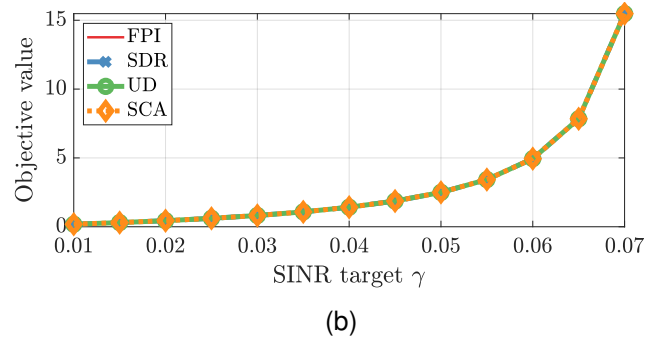
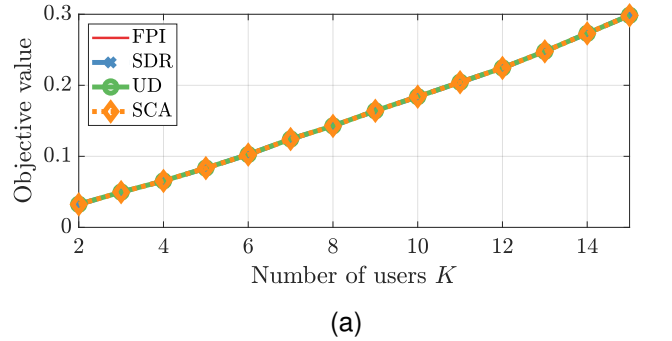


Fig. 6. (a) The objective values versus the number of users K with $\gamma = 0.01$ and $M = 8$; (b) The objective values versus the SINR target γ with $K = 10$ and $M = 8$.

B. Comparison with SOTA Algorithms

In this subsection, to illustrate the efficiency of the proposed FPI algorithm, we compare it with the following three SOTA benchmarks:

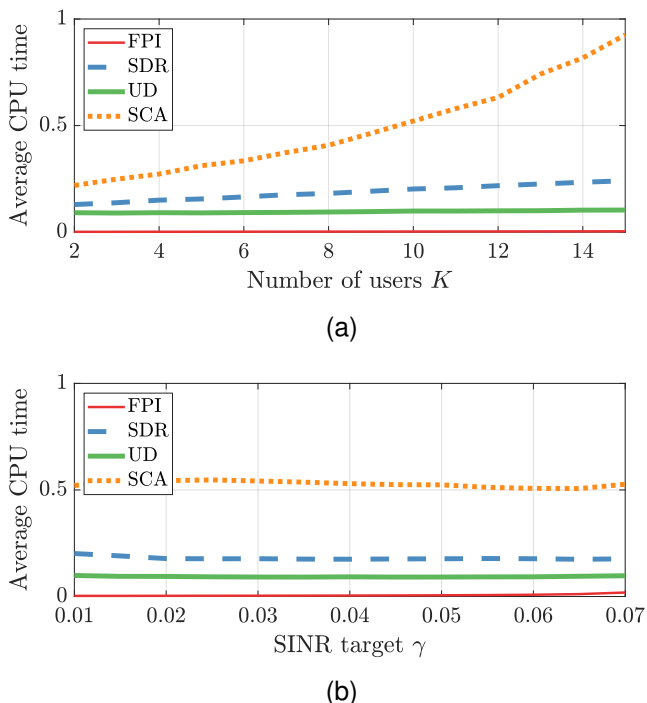


Fig. 7. (a) The average CPU time versus the number of users K with $\gamma = 0.01$ and $M = 8$; (b) The average CPU time versus the SINR target γ with $K = 10$ and $M = 8$.

- *SDR*: We call CVX [46] to directly solve the SDR in (3). This benchmark is helpful in verifying the tightness of the corresponding SDR (i.e., Theorem 1) as well as the global optimality (i.e., Theorem 3).
- *UD* [41]: The UD algorithm first uses a fixed point iteration to solve the dual uplink problem (which is obtained by transforming the Lagrangian dual problem of problem (P) with fixed beamformers); then calls CVX to solve the reduced downlink problem with fixed beamformers (which is convex). The UD algorithm is also guaranteed to find the global solution of problem (P).
- *SCA*: The SCA algorithm solves problem (P) by iteratively solving a sequence of convex approximation subproblems, and each convex approximation subproblem is obtained by linearizing the SINR constraints in problem (P) at the current point. This benchmark shows the performance when no structure of the problem is exploited. Therefore, it is useful to compare the performance gain by utilizing the special structure of the problem.

Figs. 6 and 7 show the performance comparison of the proposed FPI algorithm and the three benchmarks. In this numerical experiment, each data point is obtained by averaging over 100 channel realizations. Fig. 6 plots the average objective values of the solutions obtained by four different algorithms, where the number of users K ranges from 2 to 15 in Fig. 6(a) and the SINR target γ ranges from 0.01 to 0.07 in Fig. 6(b). We can see from Fig. 6 that all the four algorithms return the same solution. This verifies the tightness result of the SDR (i.e., Theorem 1) and the global optimality of the solution returned by the proposed algorithm (i.e., Theorem 3).

Fig. 7 plots the average CPU time taken by different

algorithms. From Fig. 7, we observe that the SCA algorithm performs the worst (even though they are initialized with a point that is close to the optimal solution). The SDR algorithm generally performs better than the SCA algorithm in terms of the CPU time. However, the CPU time of the SDR algorithm increases quickly as the number of users increases, as shown in Fig. 7(a). This is due to the fact that the SDR algorithm lifts the vector variables of the original problem to the matrix variables. On the contrary, the CPU time of the UD and FPI algorithms does not change much as the number of users increases, and both of them perform much better than the SDR algorithm. Finally, the proposed FPI algorithm significantly outperforms the UD algorithm (and the other two algorithms) in terms of the CPU time. Figs. 6 and 7 together show the global optimality and high efficiency of our proposed FPI algorithm.

The numerical results in Figs. 6 and 7 also show the importance of exploiting the problem structure in improving the solution efficiency. We make two remarks on this aspect. First, by exploiting the problem structure, we have shown the tightness of the SDR in (3), which enables us to solve the original seemingly non-convex problem (3) by solving a single convex SDR in (3). In sharp contrast, the SCA algorithm needs to solve a series of convex approximation problems to solve the original problem, which makes it less efficient than the SDR algorithm. Second, one key difference between the UD and FPI algorithms is that the proposed FPI algorithm uses the fixed point iteration in (32) to solve the primal problem while UD needs to call the solver to solve a reduced primal downlink problem (after solving the dual problem). The proposed FPI algorithm judiciously utilizes the relations between the primal and dual variables (i.e., Eqs. (6) and (12)) and hence significantly improves the computational efficiency of solving the primal problem when compared with the UD algorithm (which does not leverage the special structure of the primal problem).

VI. CONCLUSION

In this paper, we consider the QoS-based joint beamforming and compression design problem in the cooperative cellular network. A major design challenge is to find the global beamforming and compression strategy to minimize the total network transmit power. We first show in this paper, that the seemingly non-convex design problem admits a convex SDP reformulation by proving that its SDR is tight. Based on the above result, we further propose an efficient algorithm for globally solving the considered problem. The basic idea of the proposed algorithm is to solve an enhanced KKT conditions of the SDR of the considered problem via two fixed point iterations. Two key features of the proposed algorithm are: (1) it is guaranteed to find the global solution of the problem when the problem is feasible and is able to detect its infeasibility when the problem is not feasible; (2) it is highly efficient because both of fixed point iterations in the proposed algorithm are linearly convergent and each evaluation of the functions in the fixed point iterations are computationally cheap. Numerical results show that the proposed algorithm significantly outperforms the SOTA benchmarks in terms of the computational efficiency.

APPENDIX A
PROOF OF EQS. (9) AND (13)

We first prove that Eq. (9) holds at the optimal solution of the dual problem (4). Note that $\Lambda_m^{(1:m-1,1:M)}$ and $\Lambda_m^{(m:M,1:m-1)}$ do not affect the objective value or any constraints in problem (4). Hence, one can choose $\{\Lambda_m\}$ such that $\Lambda_m^{(1:m-1,1:M)}$ and $\Lambda_m^{(m:M,1:m-1)}$ are all zero. Combining the complementary slackness of \mathbf{B}_m and Λ_m with the fact that \mathbf{B}_m is of rank $M - m + 1$ or $M - m$ yields $\text{rank}(\Lambda_m) \leq 1$.

Now we prove that Eq. (13) is true. To show this, it suffices to show that the optimal dual solution $\beta_k > 0$ for all $k \in \mathcal{K}$ (due to the complementary slackness). Next, we use the following contradiction argument to show that the optimal dual solution $\beta_k > 0$ for all $k \in \mathcal{K}$. Suppose that $(\beta, \{\Lambda_m\})$ is an optimal dual solution, but there exists some k_0 such that $\beta_{k_0} = 0$. Then let $\tilde{\beta}_{k_0} = \bar{\gamma}_{k_0} \left(\mathbf{h}_{k_0}^\dagger (\mathbf{I} + \mathbf{C}_k(\beta, \{\Lambda_m\}))^{-1} \mathbf{h}_{k_0} \right)^{-1}$ and $\tilde{\beta}_k = \beta_k$ for all $k \neq k_0$. Define $\tilde{\beta} = [\tilde{\beta}_1, \tilde{\beta}_2, \dots, \tilde{\beta}_K]^\top$. Then $(\tilde{\beta}, \{\Lambda_m\})$ is a feasible dual solution with a larger objective value, which contradicts the optimality of the solution $(\beta, \{\Lambda_m\})$.

APPENDIX B
PROOF OF THEOREM 2

In this part, we shall first show the convergence of the dual fixed point iteration (24) and the primal fixed point iteration (32) by showing that both mappings $I(\cdot)$ in (23) and $J(\cdot)$ in (31) are standard interference functions [47]. Then we shall show the linear convergence rate of the dual fixed point iteration (24) and the primal fixed point iteration (32).

A. Convergence of Fixed Point Iterations (24) and (32)

From Theorem 2 in [47], to show the convergence of fixed point iterations (24) and (32), it suffices to show that both mappings $I(\cdot)$ in (23) and $J(\cdot)$ in (31) are standard interference functions [47]. The mapping $f : \mathbb{R}_+^n \rightarrow \mathbb{R}_+^n$ is said to be a standard interference function if it satisfies the following three properties.

Positivity: For any $\mathbf{x} \in \mathbb{R}_+^n$, $f(\mathbf{x}) \geq \mathbf{0}$.

Strict sub-homogeneity: For any $\alpha > 1$ and $\mathbf{x} \in \mathbb{R}_+^n \setminus \{\mathbf{0}\}$, $f(\alpha\mathbf{x}) < \alpha f(\mathbf{x})$.

Monotonicity: For any $\mathbf{x}_1, \mathbf{x}_2 \in \mathbb{R}_+^n$ with $\mathbf{x}_1 \geq \mathbf{x}_2$, $f(\mathbf{x}_1) \geq f(\mathbf{x}_2)$.

Notice that a mapping $f = [f_1, f_2, \dots, f_n]^\top$ is a standard interference function if and only if all of its components f_i satisfy the above three properties.

1) $I(\cdot)$ in (23) is a standard interference function: We show that $I(\cdot)$ in (23) is a standard interference function by showing that $I_k(\cdot)$ in (22) for all $k \in \mathcal{K}$ satisfy the positivity, the strict sub-homogeneity, and the monotonicity one by one. From (22), for any $k \in \mathcal{K}$, we have

$$I_k(\beta) = \frac{\bar{\gamma}_k}{\mathbf{h}_k^\dagger (\mathbf{I} + \mathbf{C}_k(\beta))^{-1} \mathbf{h}_k}, \quad (37)$$

where we use $\mathbf{C}_k(\beta)$ to denote

$$\mathbf{C}_k(\beta, \{\Lambda_m(\beta)\}) = \sum_{m \in \mathcal{M}} \Lambda_m^{(m,m)}(\beta) \mathbf{E}_m + \sum_{j \neq k} \beta_j \mathbf{H}_j \quad (38)$$

to simplify the notations. In the following, we shall show the desired properties of $I_k(\cdot)$ based on the properties of $\Lambda_m^{(m,m)}(\cdot)$ in Lemma 5 given in Appendix D-A of the Supplementary Material.

Proof of the positivity of $I_k(\cdot)$: For any $m \in \mathcal{M}$, $\Lambda_m^{(m,m)}(\cdot)$ is positive by Lemma 5, which implies that $\mathbf{I} + \mathbf{C}_k(\beta)$ is positive definite for any $\beta \in \mathbb{R}_+^K$. Hence, by (37), $I_k(\cdot)$ is positive.

Proof of the strict sub-homogeneity of $I_k(\cdot)$: For any $\alpha > 1$ and $\beta \in \mathbb{R}_+^K \setminus \{\mathbf{0}\}$, it follows from the strict sub-homogeneity of $\Lambda_m^{(m,m)}(\cdot)$ in Lemma 5 and (38) that

$$\begin{aligned} \mathbf{C}_k(\alpha\beta) &= \sum_{m \in \mathcal{M}} \Lambda_m^{(m,m)}(\alpha\beta) \mathbf{E}_m + \sum_{j \neq k} \alpha\beta_j \mathbf{H}_j \\ &< \alpha \left(\sum_{m \in \mathcal{M}} \Lambda_m^{(m,m)}(\beta) \mathbf{E}_m + \sum_{j \neq k} \beta_j \mathbf{H}_j \right) \\ &= \alpha \mathbf{C}_k(\beta). \end{aligned} \quad (39)$$

As such, by (37), we get

$$\begin{aligned} I_k(\alpha\beta) &= \bar{\gamma}_k \left(\mathbf{h}_k^\dagger (\mathbf{I} + \mathbf{C}_k(\alpha\beta))^{-1} \mathbf{h}_k \right)^{-1} \\ &< \bar{\gamma}_k \left(\mathbf{h}_k^\dagger (\alpha\mathbf{I} + \alpha\mathbf{C}_k(\beta))^{-1} \mathbf{h}_k \right)^{-1} \\ &= \alpha I_k(\beta). \end{aligned}$$

Proof of the monotonicity of $I_k(\cdot)$: For any $\beta_1, \beta_2 \in \mathbb{R}_+^K$ with $\beta_\ell = [\beta_{\ell,1}, \beta_{\ell,2}, \dots, \beta_{\ell,K}]^\top$ for $\ell = 1, 2$ and $\beta_1 \geq \beta_2$, the monotonicity of $\Lambda_m^{(m,m)}(\cdot)$ in Lemma 5 and (38) gives

$$\begin{aligned} \mathbf{C}_k(\beta_2) &= \sum_{m \in \mathcal{M}} \Lambda_m^{(m,m)}(\beta_2) \mathbf{E}_m + \sum_{j \neq k} \beta_{2,j} \mathbf{H}_j \\ &\preceq \sum_{m \in \mathcal{M}} \Lambda_m^{(m,m)}(\beta_1) \mathbf{E}_m + \sum_{j \neq k} \beta_{1,j} \mathbf{H}_j \\ &= \mathbf{C}_k(\beta_1). \end{aligned}$$

Combining this with (37) yields

$$\begin{aligned} I_k(\beta_2) &= \bar{\gamma}_k \left(\mathbf{h}_k^\dagger (\mathbf{I} + \mathbf{C}_k(\beta_2))^{-1} \mathbf{h}_k \right)^{-1} \\ &\leq \bar{\gamma}_k \left(\mathbf{h}_k^\dagger (\mathbf{I} + \mathbf{C}_k(\beta_1))^{-1} \mathbf{h}_k \right)^{-1} \\ &= I_k(\beta_1). \end{aligned}$$

2) $J(\cdot)$ in (31) is a standard interference function: We show the positivity, the strict sub-homogeneity, and the monotonicity of $J_k(\cdot)$ one by one, where $J_k(\cdot)$ in (30) can be explicitly written as

$$J_k(\mathbf{p}) = \frac{\bar{\gamma}_k \left(\sum_{j \neq k} p_j \text{tr} \left(\hat{\mathbf{V}}_j \mathbf{H}_k \right) + \text{tr}(\mathbf{Q}(\mathbf{p}) \mathbf{H}_k) + \sigma_k^2 \right)}{\text{tr} \left(\hat{\mathbf{V}}_k \mathbf{H}_k \right)}. \quad (40)$$

In the following, we shall show the desired properties of $J_k(\cdot)$ based on the properties of $\mathbf{Q}(\cdot)$ in Lemma 6 given in Appendix D-B of the Supplementary Material.

Proof of the positivity of $J_k(\cdot)$: For any $\mathbf{p} \in \mathbb{R}_+^K$, the non-negativity of $\mathbf{Q}(\cdot)$ in Lemma 6 and (40) yields

$$J_k(\mathbf{p}) \geq \frac{\bar{\gamma}_k \sigma_k^2}{\text{tr} \left(\hat{\mathbf{V}}_k \mathbf{H}_k \right)} > 0.$$

Proof of the strict sub-homogeneity of $J_k(\cdot)$: For any $\alpha > 1$ and $\mathbf{p} \in \mathbb{R}_+^K \setminus \{\mathbf{0}\}$, the linearity of $\mathbf{Q}(\cdot)$ in Lemma 6 together with (40) gives

$$\begin{aligned} J_k(\alpha\mathbf{p}) &= \frac{\bar{\gamma}_k \left(\alpha \sum_{j \neq k} p_j \text{tr} \left(\hat{\mathbf{V}}_j \mathbf{H}_k \right) + \alpha \text{tr} \left(\mathbf{Q}(\mathbf{p}) \mathbf{H}_k \right) + \sigma_k^2 \right)}{\text{tr} \left(\hat{\mathbf{V}}_k \mathbf{H}_k \right)} \\ &< \frac{\bar{\gamma}_k \left(\alpha \sum_{j \neq k} p_j \text{tr} \left(\hat{\mathbf{V}}_j \mathbf{H}_k \right) + \alpha \text{tr} \left(\mathbf{Q}(\mathbf{p}) \mathbf{H}_k \right) + \alpha \sigma_k^2 \right)}{\text{tr} \left(\hat{\mathbf{V}}_k \mathbf{H}_k \right)} \\ &= \alpha J_k(\mathbf{p}). \end{aligned}$$

Proof of the monotonicity of $J_k(\cdot)$: For any $\mathbf{p}_1, \mathbf{p}_2 \in \mathbb{R}_+^K$ with $\mathbf{p}_1 \geq \mathbf{p}_2$, combining the monotonicity of $\mathbf{Q}(\cdot)$ in Lemma 6 and (40) shows that

$$\begin{aligned} J_k(\mathbf{p}_2) &= \frac{\bar{\gamma}_k \left(\sum_{j \neq k} p_{1,j} \text{tr} \left(\hat{\mathbf{V}}_j \mathbf{H}_k \right) + \text{tr} \left(\mathbf{Q}(\mathbf{p}_2) \mathbf{H}_k \right) + \sigma_k^2 \right)}{\text{tr} \left(\hat{\mathbf{V}}_k \mathbf{H}_k \right)} \\ &\leq \frac{\bar{\gamma}_k \left(\sum_{j \neq k} p_{2,j} \text{tr} \left(\hat{\mathbf{V}}_j \mathbf{H}_k \right) + \text{tr} \left(\mathbf{Q}(\mathbf{p}_1) \mathbf{H}_k \right) + \sigma_k^2 \right)}{\text{tr} \left(\hat{\mathbf{V}}_k \mathbf{H}_k \right)} \\ &= J_k(\mathbf{p}_1). \end{aligned}$$

B. Linear Convergence Rates of Fixed Point Iterations (24) and (32)

In this part, we show the linear convergence rate of both iterations. First, combining the linearity of $\mathbf{Q}(\cdot)$ in Lemma 6 and (40) gives that $J(\cdot)$ is an affine function. Hence, the convergence of the primal fixed point iteration (32) immediately implies its linear convergence rate (and the rate depends on the spectral radius of matrix \mathbf{G} whose entries are given in (36)). Next, we shall focus on showing the linear convergence rate of the dual fixed point iteration (24). To this end, we need the following two lemmas. Recall the metric $\mu(\cdot, \cdot)$ defined in (33).

Lemma 1: For any $\beta, \gamma \in \mathbb{R}_{++}^K$, we have

$$\frac{\mu(I(\beta), I(\gamma))}{\mu(\beta, \gamma)} \leq \max_k \left\{ \log_\alpha \left(\frac{I_k(\alpha\gamma)}{I_k(\gamma)} \right), \log_\alpha \left(\frac{I_k(\alpha\beta)}{I_k(\beta)} \right) \right\}, \quad (41)$$

where $\alpha = e^{\mu(\beta, \gamma)}$.

Proof: By the definition of $\mu(\cdot, \cdot)$ in (33), we get $\beta \leq \alpha\gamma$ and $\gamma \leq \alpha\beta$. Combining this with the monotonicity of $I_k(\cdot)$ gives

$$I_k(\beta) \leq I_k(\alpha\gamma) \text{ and } I_k(\gamma) \leq I_k(\alpha\beta).$$

As a result,

$$\begin{aligned} \mu(I(\beta), I(\gamma)) &= \max_k \left| \log \left(\frac{I_k(\beta)}{I_k(\gamma)} \right) \right| \\ &\leq \max_k \left\{ \log \left(\frac{I_k(\alpha\gamma)}{I_k(\gamma)} \right), \log \left(\frac{I_k(\alpha\beta)}{I_k(\beta)} \right) \right\}. \end{aligned}$$

Dividing both sides of the above inequality by $\mu(\beta, \gamma)$ yields the desired result (41). \square

Lemma 2: For any $\alpha > 1$ and $\beta \in \mathbb{R}_{++}^K$, we have

$$\log_\alpha \left(\frac{I_k(\alpha\beta)}{I_k(\beta)} \right) < \log_\alpha \left(\frac{1 + \alpha \lambda_1^k(\beta)}{1 + \lambda_1^k(\beta)} \right), \quad (42)$$

where we use $\lambda_1^k(\beta)$ to denote $\|\mathbf{C}_k(\beta)\|_2$.

Proof: For any $\alpha > 1$ and $\beta \in \mathbb{R}_{++}^K$, it follows from (37) and (39) that

$$\begin{aligned} \frac{I_k(\alpha\beta)}{I_k(\beta)} &= \frac{\mathbf{h}_k^\dagger (\mathbf{I} + \mathbf{C}_k(\beta))^{-1} \mathbf{h}_k}{\mathbf{h}_k^\dagger (\mathbf{I} + \mathbf{C}_k(\alpha\beta))^{-1} \mathbf{h}_k} \\ &< \frac{\mathbf{h}_k^\dagger (\mathbf{I} + \mathbf{C}_k(\beta))^{-1} \mathbf{h}_k}{\mathbf{h}_k^\dagger (\mathbf{I} + \alpha \mathbf{C}_k(\beta))^{-1} \mathbf{h}_k}. \end{aligned} \quad (43)$$

In the rest part of the proof, we drop the dependence of all variables on β and k for notational simplicity. Suppose $\mathbf{U}\mathbf{\Lambda}\mathbf{U}^\dagger$ is the spectral decomposition of \mathbf{C} , where $\mathbf{\Lambda} = \text{diag}(\lambda_1, \lambda_2, \dots, \lambda_M)$ with decreasing λ_m . Let $\mathbf{v} = \mathbf{U}^\dagger \mathbf{h} = [v_1, v_2, \dots, v_M]^\top$. Then, we get

$$\begin{aligned} \frac{\mathbf{h}^\dagger (\mathbf{I} + \mathbf{C})^{-1} \mathbf{h}}{\mathbf{h}^\dagger (\mathbf{I} + \alpha \mathbf{C})^{-1} \mathbf{h}} &= \frac{\mathbf{v}^\dagger (\mathbf{I} + \mathbf{\Lambda})^{-1} \mathbf{v}}{\mathbf{v}^\dagger (\mathbf{I} + \alpha \mathbf{\Lambda})^{-1} \mathbf{v}} \\ &= \frac{\sum_{m \in \mathcal{M}} \frac{1}{1 + \lambda_m} |v_m|^2}{\sum_{m \in \mathcal{M}} \frac{1}{1 + \alpha \lambda_m} |v_m|^2} \\ &\leq \frac{\sum_{m \in \mathcal{M}} \frac{1}{1 + \lambda_1} |v_m|^2}{\sum_{m \in \mathcal{M}} \frac{1}{1 + \alpha \lambda_1} |v_m|^2} \\ &= \frac{1 + \alpha \lambda_1}{1 + \lambda_1}. \end{aligned} \quad (44)$$

Finally, combining (43) and (44) and taking the α -logarithm from both sides yield the desired result (42). \square

Define $\kappa(\alpha, \lambda) = \log_\alpha \left(\frac{1 + \alpha \lambda}{1 + \lambda} \right)$. Then it is simple to verify that the function has the following properties:

- (i) $\kappa(\alpha, \lambda)$ is an increasing function of both α and λ ;
- (ii) $\kappa(\alpha, \lambda) \in (0, 1)$ for any $\alpha > 1$ and $\lambda > 0$; and
- (iii) $\lim_{\alpha \rightarrow \infty} \kappa(\alpha, \lambda) = \frac{\lambda}{1 + \lambda}$ for any $\lambda > 0$.

Now, we are ready to show the linear convergence rate of the dual fixed point iteration (24). First, substituting β and γ with $\beta^{(i)}$ and β^* in Lemma 1 and using Lemma 2 gives

$$\frac{\mu(\beta^{(i+1)}, \beta^*)}{\mu(\beta^{(i)}, \beta^*)} < \max_k \left\{ \kappa(\alpha_i, \lambda_1^k(\beta^{(i)})), \kappa(\alpha_i, \lambda_1^k(\beta^*)) \right\},$$

where $\alpha_i = e^{\mu(\beta^{(i)}, \beta^*)}$. Since $\kappa(\alpha, \cdot)$ is an increasing function, it follows from the fact $\lambda(\beta) = \max_k \{\lambda_1^k(\beta)\}$ that

$$\frac{\mu(\beta^{(i+1)}, \beta^*)}{\mu(\beta^{(i)}, \beta^*)} < \max \left\{ \kappa(\alpha_i, \lambda(\beta^{(i)})), \kappa(\alpha_i, \lambda(\beta^*)) \right\}. \quad (45)$$

Taking the limit superior on both sides of (45) and using the properties of $\kappa(\cdot, \cdot)$, we obtain

$$\begin{aligned} \limsup_{i \rightarrow \infty} \frac{\mu(\beta^{(i+1)}, \beta^*)}{\mu(\beta^{(i)}, \beta^*)} &\leq \max \left\{ \lim_{i \rightarrow \infty} \kappa(\alpha_i, \lambda(\beta^{(i)})), \lim_{i \rightarrow \infty} \kappa(\alpha_i, \lambda(\beta^*)) \right\} \\ &= \frac{\lambda(\beta^*)}{1 + \lambda(\beta^*)}. \end{aligned}$$

This shows the (asymptotic) linear convergence rate of the dual fixed point iteration (24) given in (34).

REFERENCES

- [1] X. Fan, Y.-F. Liu, and L. Liu, "Efficiently and globally solving joint beamforming and compression problem in the cooperative cellular network via Lagrangian duality," in *Proc. IEEE ICASSP*, May 2022, pp. 5388–5392.
- [2] S. Boyd, S. P. Boyd, and L. Vandenberghe, *Convex Optimization*. Cambridge University Press, 2004.
- [3] F. Rashid-Farrokh, K. R. Liu, and L. Tassiulas, "Transmit beamforming and power control for cellular wireless systems," *IEEE J. Sel. Areas Commun.*, vol. 16, no. 8, pp. 1437–1450, Oct. 1998.
- [4] H. Boche and M. Schubert, "A general duality theory for uplink and downlink beamforming," in *Proc. IEEE 56th Veh. Technol. Conf. (VTC)*, vol. 1, Sep. 2002, pp. 87–91 vol.1.
- [5] M. Schubert and H. Boche, "Solution of the multiuser downlink beamforming problem with individual SINR constraints," *IEEE Trans. Veh. Technol.*, vol. 53, no. 1, pp. 18–28, Jan. 2004.
- [6] A. Wiesel, Y. Eldar, and S. Shamai, "Linear precoding via conic optimization for fixed MIMO receivers," *IEEE Trans. Signal Process.*, vol. 54, no. 1, pp. 161–176, Jan. 2006.
- [7] P. Viswanath and D. Tse, "Sum capacity of the vector Gaussian broadcast channel and uplink–downlink duality," *IEEE Trans. Inf. Theory*, vol. 49, no. 8, pp. 1912–1921, Aug. 2003.
- [8] B. Song, R. L. Cruz, and B. D. Rao, "Network duality for multiuser MIMO beamforming networks and applications," *IEEE Trans. Commun.*, vol. 55, no. 3, pp. 618–630, Mar. 2007.
- [9] W. Yu, "Uplink–downlink duality via minimax duality," *IEEE Trans. Inf. Theory*, vol. 52, no. 2, pp. 361–374, Feb. 2006.
- [10] E. Visotsky and U. Madhow, "Optimum beamforming using transmit antenna arrays," in *Proc. IEEE 49th Veh. Technol. Conf. (VTC)*, vol. 1, 1999, pp. 851–856.
- [11] F. Rashid-Farrokh, L. Tassiulas, and K. R. Liu, "Joint optimal power control and beamforming in wireless networks using antenna arrays," *IEEE Trans. Commun.*, vol. 46, no. 10, pp. 1313–1324, Oct. 1998.
- [12] S. Vishwanath, N. Jindal, and A. Goldsmith, "Duality, achievable rates, and sum-rate capacity of Gaussian MIMO broadcast channels," *IEEE Trans. Inf. Theory*, vol. 49, no. 10, pp. 2658–2668, Oct. 2003.
- [13] M. Bengtsson and B. Ottersten, "Optimum and suboptimum transmit beamforming," in *Handbook of Antennas in Wireless Communications*. CRC Press, 2002, p. 34.
- [14] M. Schubert and H. Boche, "Iterative multiuser uplink and downlink beamforming under SINR constraints," *IEEE Trans. Signal Process.*, vol. 53, no. 7, pp. 2324–2334, Jul. 2005.
- [15] D. W. H. Cai, T. Q. S. Quek, C. W. Tan, and S. H. Low, "Max-min weighted SINR in coordinated multicell MIMO downlink," in *Proc. IEEE Int. Symp. Model Optim. Mobile Ad Hoc Wireless Netw. (WiOpt)*, May 2011, pp. 286–293.
- [16] W. Yu and T. Lan, "Transmitter optimization for the multi-antenna downlink with per-antenna power constraints," *IEEE Trans. Signal Process.*, vol. 55, no. 6, pp. 2646–2660, Jun. 2007.
- [17] D. Hammarwall, M. Bengtsson, and B. Ottersten, "On downlink beamforming with indefinite shaping constraints," *IEEE Trans. Signal Process.*, vol. 54, no. 9, pp. 3566–3580, Sep. 2006.
- [18] H. Dahrouj and W. Yu, "Coordinated beamforming for the multicell multi-antenna wireless system," *IEEE Trans. Wireless Commun.*, vol. 9, no. 5, pp. 1748–1759, May 2010.
- [19] R. Irmer, H. Droste, P. Marsch, M. Grieger, G. Fettweis, S. Brueck, H.-P. Mayer, L. Thiele, and V. Jungnickel, "Coordinated multipoint: Concepts, performance, and field trial results," *IEEE Commun. Mag.*, vol. 49, no. 2, pp. 102–111, Feb. 2011.
- [20] K. Kerpez, "A radio access system with distributed antennas," *IEEE Trans. Veh. Technol.*, vol. 45, no. 2, pp. 265–275, May 1996.
- [21] O. Simeone, A. Maeder, M. Peng, O. Sahin, and W. Yu, "Cloud radio access network: Virtualizing wireless access for dense heterogeneous systems," *J. Commun. Netw.*, vol. 18, no. 2, pp. 135–149, Apr. 2016.
- [22] H. Q. Ngo, A. Ashikhmin, H. Yang, E. G. Larsson, and T. L. Marzetta, "Cell-free massive MIMO versus small cells," *IEEE Trans. Wireless Commun.*, vol. 16, no. 3, pp. 1834–1850, Mar. 2017.
- [23] M. Peng, C. Wang, V. Lau, and H. V. Poor, "Fronthaul-constrained cloud radio access networks: Insights and challenges," *IEEE Wireless Commun.*, vol. 22, no. 2, pp. 152–160, Apr. 2015.
- [24] B. Dai and W. Yu, "Sparse beamforming and user-centric clustering for downlink cloud radio access network," *IEEE Access*, vol. 2, pp. 1326–1339, 2014.
- [25] Y. Shi, J. Zhang, and K. B. Letaief, "Group sparse beamforming for green cloud-RAN," *IEEE Trans. Wireless Commun.*, vol. 13, no. 5, pp. 2809–2823, May 2014.
- [26] S.-H. Park, O. Simeone, O. Sahin, and S. Shamai, "Joint precoding and multivariate backhaul compression for the downlink of cloud radio access networks," *IEEE Trans. Signal Process.*, vol. 61, no. 22, pp. 5646–5658, Nov. 2013.
- [27] —, "Inter-cluster design of precoding and fronthaul compression for cloud radio access networks," *IEEE Wireless Commun. Lett.*, vol. 3, no. 4, pp. 369–372, Aug. 2014.
- [28] Y. Jeon, S.-H. Park, C. Song, J. Moon, S. Maeng, and I. Lee, "Joint designs of fronthaul compression and precoding for full-duplex cloud radio access networks," *IEEE Wireless Commun. Lett.*, vol. 5, no. 6, pp. 632–635, Dec. 2016.
- [29] W. Tang and S. Feng, "User selection and power minimization in full-duplex cloud radio access networks," *IEEE Trans. Signal Process.*, vol. 67, no. 9, pp. 2426–2438, May 2019.
- [30] P. Patil and W. Yu, "Hybrid compression and message-sharing strategy for the downlink cloud radio-access network," in *Proc. Inf. Theory Appl. Workshop (ITA)*, Feb. 2014, pp. 1–6.
- [31] J. Kang, O. Simeone, J. Kang, and S. Shamai, "Fronthaul compression and precoding design for C-RANs over ergodic fading channels," *IEEE Trans. Veh. Technol.*, vol. 65, no. 7, pp. 5022–5032, Jul. 2016.
- [32] S. He, Y. Wu, J. Ren, Y. Huang, R. Schober, and Y. Zhang, "Hybrid precoder design for cache-enabled millimeter-wave radio access networks," *IEEE Trans. Wireless Commun.*, vol. 18, no. 3, pp. 1707–1722, Mar. 2019.
- [33] J. Kim, S.-H. Park, O. Simeone, I. Lee, and S. S. Shitz, "Joint design of fronthauling and hybrid beamforming for downlink C-RAN systems," *IEEE Trans. Commun.*, vol. 67, no. 6, pp. 4423–4434, Jun. 2019.
- [34] S. Ahn, S.-I. Park, J.-Y. Lee, N. Hur, and J. Kang, "Fronthaul compression and precoding optimization for NOMA-based joint transmission of broadcast and unicast services in C-RAN," *IEEE Trans. Broadcast.*, vol. 66, no. 4, pp. 786–799, Dec. 2020.
- [35] Y. Zhang, X. Wu, H. Peng, C. Zhong, and X. Chen, "Beamforming and fronthaul compression design for intelligent reflecting surface aided cloud radio access networks," *Front. Inform. Technol. Electron. Eng.*, vol. 23, no. 1, pp. 31–46, Jan. 2022.
- [36] Y. Huang and A. Ikhlef, "Joint optimization of wireless fronthaul and access links in CRAN with a massive MIMO central unit," in *Proc. IEEE Int. Conf. Commun. (ICC)*, May 2022, pp. 1906–1911.
- [37] D. Maryopi, Y. Huang, and A. Ikhlef, "Sum-rate maximization in uplink CRAN with a massive MIMO fronthaul," in *Proc. IEEE Global Commun. Conf. (GLOBECOM)*, Dec. 2021, pp. 1–6.
- [38] Y. Zhou and W. Yu, "Fronthaul compression and transmit beamforming optimization for multi-antenna uplink C-RAN," *IEEE Trans. Signal Process.*, vol. 64, no. 16, pp. 4138–4151, Aug. 2016.
- [39] U. Krause, "Perron's stability theorem for non-linear mappings," *J. Math. Economics*, vol. 15, no. 3, pp. 275–282, Jan. 1986.
- [40] L. Liu, P. Patil, and W. Yu, "An uplink–downlink duality for cloud radio access network," in *Proc. IEEE Int. Symp. Inf. Theory (ISIT)*, Jul. 2016, pp. 1606–1610.
- [41] L. Liu, Y.-F. Liu, P. Patil, and W. Yu, "Uplink–downlink duality between multiple-access and broadcast channels with compressing relays," *IEEE Trans. Inf. Theory*, pp. 7304–7337, Nov. 2021.
- [42] Z.-Q. Luo, W.-K. Ma, A. So, Y. Ye, and S. Zhang, "Semidefinite relaxation of quadratic optimization problems," *IEEE Signal Process. Mag.*, vol. 27, no. 3, pp. 20–34, May 2010.
- [43] C. Lu, Y.-F. Liu, W.-Q. Zhang, and S. Zhang, "Tightness of a new and enhanced semidefinite relaxation for MIMO detection," *SIAM J. Optim.*, vol. 29, no. 1, pp. 719–742, Jan. 2019.
- [44] F. Liu, Y.-F. Liu, A. Li, C. Masouros, and Y. C. Eldar, "Cramér-Rao bound optimization for joint radar-communication beamforming," *IEEE Trans. Signal Process.*, vol. 70, pp. 240–253, 2022.
- [45] C. J. Nuzman, "Contraction approach to power control, with non-monotonic applications," in *Proc. IEEE Global Commun. Conf. (GLOBECOM)*, Nov. 2007, pp. 5283–5287.
- [46] M. Grant and S. Boyd, "CVX: Matlab software for disciplined convex programming, version 2.1," <http://cvxr.com/cvx>, Mar. 2014.
- [47] R. Yates, "A framework for uplink power control in cellular radio systems," *IEEE J. Sel. Areas Commun.*, vol. 13, no. 7, pp. 1341–1347, Sep. 1995.
- [48] F. Zhang, Ed., *The Schur Complement and Its Applications*. New York: Springer, 2005.

Supplementary Material

In this supplementary material, for the convenience of the presentation, we sometimes denote $\Gamma_m(\beta)$ by Γ_m , denote $\Lambda_m(\beta)$ by Λ_m , and denote $\mathbf{Q}(\beta)$ by \mathbf{Q} . Besides, consider the cone \mathcal{C} , which can either be the non-negative orthant \mathbb{R}_+^n or the positive semidefinite matrix cone \mathcal{S}_+^n . The order relationship $\succeq_{\mathcal{C}}$ ($\succ_{\mathcal{C}}$) denotes \geq ($>$) if $\mathcal{C} = \mathbb{R}_+^n$ and denotes \succeq (\succ) if $\mathcal{C} = \mathcal{S}_+^n$. Given two cones \mathcal{C}_1 and \mathcal{C}_2 , a mapping $f : \mathcal{C}_1 \rightarrow \mathcal{C}_2$ is called

- (i) concave if $f(\lambda \mathbf{A}_1 + (1 - \lambda) \mathbf{A}_2) \succeq_{\mathcal{C}_2} \lambda f(\mathbf{A}_1) + (1 - \lambda) f(\mathbf{A}_2)$ for all $\mathbf{A}_1, \mathbf{A}_2 \succ_{\mathcal{C}_1} \mathbf{0}$ and $\lambda \in [0, 1]$;
- (ii) homogeneous if $f(\lambda \mathbf{A}) = \lambda f(\mathbf{A})$ for all $\mathbf{A} \succ_{\mathcal{C}_1} \mathbf{0}$ and $\lambda > 0$;
- (iii) non-negative if $f(\mathbf{A}) \succeq_{\mathcal{C}_2} \mathbf{0}$ for all $\mathbf{A} \succeq_{\mathcal{C}_1} \mathbf{0}$;
- (iv) strictly non-negative if $f(\mathbf{A}) \succ_{\mathcal{C}_2} \mathbf{0}$ for all $\mathbf{A} \succ_{\mathcal{C}_1} \mathbf{0}$;
- (v) monotonic if $f(\mathbf{A}_1) \succeq_{\mathcal{C}_2} f(\mathbf{A}_2)$ for all $\mathbf{A}_1, \mathbf{A}_2 \succeq_{\mathcal{C}_1} \mathbf{0}$ with $\mathbf{A}_1 \succeq_{\mathcal{C}_1} \mathbf{A}_2$; and
- (vi) strictly monotonic if $f(\mathbf{A}_1) \succ_{\mathcal{C}_2} f(\mathbf{A}_2)$ for all $\mathbf{A}_1, \mathbf{A}_2 \succ_{\mathcal{C}_1} \mathbf{0}$ with $\mathbf{A}_1 \succ_{\mathcal{C}_1} \mathbf{A}_2$.

Note that the above definition of the monotonicity coincides with the definition given in Appendix B when f maps \mathbb{R}_+^K to \mathbb{R}_+^K .

APPENDIX C

DETAILS ON SOLVING EQS. (8) AND (9) FOR $\{\Lambda_m\}$

In this part, we shall provide more details on solving Eqs. (8) and (9) for $\{\Lambda_m\}$. For any positive integer n and any $\eta > 1$, define the mapping $S_\eta : \mathcal{S}_{++}^n \rightarrow \mathcal{S}_{++}^{n-1}$ by

$$S_\eta(\Gamma) = \Gamma^{(2:n,2:n)} - \frac{\Gamma^{(2:n,1)} \Gamma^{(1,2:n)}}{\frac{\eta}{\eta-1} \Gamma^{(1,1)}}. \quad (46)$$

Let $\Gamma_1 = \Gamma(\beta)$, where $\Gamma(\cdot)$ is defined in (16). Then by the described procedure in Section IV-A1, Γ_{m+1} is given by

$$\Gamma_{m+1} = \begin{bmatrix} \mathbf{0} & \mathbf{0} \\ \mathbf{0} & S_{\bar{\eta}_m} \left(\Gamma_m^{(m:M,m:M)} \right) \end{bmatrix}. \quad (47)$$

Once $\{\Gamma_m\}$ are computed, we can obtain $\{\Lambda_m\}$ based on (20), and in particular,

$$\Lambda_m^{(m,m)} = \frac{1}{\bar{\eta}_m - 1} \Gamma_m^{(m,m)}. \quad (48)$$

Based on the recursive formula (47) and (48), we have that, for any $m \in \mathcal{M}$,

$$\Lambda_m^{(m,m)}(\beta) = \frac{1}{\bar{\eta}_m - 1} ((T_m \circ \Gamma)(\beta))^{(1,1)}, \quad (49)$$

where we define

$$T_m = \begin{cases} S_{\bar{\eta}_{m-1}} \circ \dots \circ S_{\eta_1}, & \text{if } m = 2, 3, \dots, M, \\ \text{identity mapping}, & \text{if } m = 1. \end{cases} \quad (50)$$

As will be seen later, (49) is useful for the analysis of the properties of $\{\Lambda_m^{(m,m)}(\cdot)\}$ in Appendix D-A.

APPENDIX D

USEFUL PROPERTIES OF $\{\Lambda_m^{(m,m)}(\cdot)\}$ AND $\mathbf{Q}(\cdot)$

In this part, we shall derive some useful properties of $\{\Lambda_m^{(m,m)}(\cdot)\}$ and $\mathbf{Q}(\cdot)$, which play central roles in showing that $I(\cdot)$ in (23) and $J(\cdot)$ in (31) are standard interference functions [47], respectively.

A. Useful Properties of $\{\Lambda_m^{(m,m)}(\cdot)\}$

We shall first study the properties of the obtained components $\{\Lambda_m^{(m,m)}(\cdot)\}$ in (49). As shown in (49), $\Lambda_m^{(m,m)}(\cdot)$ is a composition of $\{S_{\bar{\eta}_m}(\cdot)\}$ and $\Gamma(\cdot)$ in (16). Hence, to study the properties of $\Lambda_m^{(m,m)}(\cdot)$, we need to first study the properties of $S_\eta(\cdot)$ in (46).

For any $\eta > 1$, $S_\eta(\cdot)$ in (46) can be equivalently rewritten as

$$S_\eta(\Gamma) = \frac{\eta - 1}{\eta} \Gamma^{(1:n,1:n)} / \Gamma^{(1,1)} + \frac{1}{\eta} \Gamma^{(2:n,2:n)},$$

which is a convex combination of a Schur complement and a linear part of Γ . The concavity and homogeneity of $S_\eta(\cdot)$ come from the concavity and homogeneity of the Schur complement [2, Exercise 3.58]. Moreover, $S_\eta(\cdot)$ is also strictly non-negative. Finally, we have the following lemma on the monotonicity of $S_\eta(\cdot)$.

Lemma 3: For a concave and homogeneous mapping $f : \mathcal{C}_1 \rightarrow \mathcal{C}_2$, the following holds.

- (i) If f is non-negative, then it is monotonic. In particular, this conclusion holds when f is linear and non-negative.
- (ii) If f is strictly non-negative, then it is strictly monotonic.

Proof: For any $\mathbf{A}_1, \mathbf{A}_2 \succeq_{\mathcal{C}_1} \mathbf{0}$ such that $\mathbf{A}_1 \succeq_{\mathcal{C}_1} \mathbf{A}_2$, we have

$$f(\mathbf{A}_1) \succeq_{\mathcal{C}_2} f(\mathbf{A}_2) + f(\mathbf{A}_1 - \mathbf{A}_2) \succeq_{\mathcal{C}_2} f(\mathbf{A}_2),$$

where the first inequality follows from the concavity and homogeneity of f , and the second inequality follows from the non-negativity of f . When f is strictly non-negative, the proof can be done analogously by replacing \succeq in the conditions and the second inequality with \succ . \square

Next, we shall study the properties of the composite mapping T_m in (50).

Lemma 4: If f and g are two concave, homogeneous, and strictly non-negative mappings, so does their composition $f \circ g$.

Proof: From Lemma 3, we know that f is monotonically increasing. Since g is concave, and f is concave and non-decreasing, their composition $f \circ g$ is concave [2, Chapter 3]. Besides, the homogeneity and strict non-negativity of the composition $f \circ g$ is obvious. \square

The concavity, the homogeneity, and the strict non-negativity of T_m in (50) come from the following induction argument. First, $T_2 = S_{\eta_1}$ is concave, homogeneous, and strictly non-negative. Lemma 4 shows that if T_{m-1} and $S_{\bar{\eta}_{m-1}}$ have these properties, then $T_m = S_{\bar{\eta}_{m-1}} \circ T_{m-1}$ also has these properties. Hence, for any $m \in \mathcal{M}$, T_m is concave, homogeneous, and strictly non-negative. Furthermore, the strict monotonicity of $T_m(\cdot)$ follows from Lemma 3.

Now, we present the nice properties of $\{\Lambda_m^{(m,m)}(\cdot)\}$ in the following Lemma 5.

Lemma 5: For any $m \in \mathcal{M}$, $\Lambda_m^{(m,m)}(\cdot)$ in (49) is positive, strictly sub-homogeneous, and monotonic.

Proof: We prove these properties of $\Lambda_m^{(m,m)}(\cdot)$ one by one.

Positivity: For any $\beta \in \mathbb{R}_+^K$, we have $\Gamma(\beta) \succeq \mathbf{I} \succ \mathbf{0}$ by (16). Therefore, the strict non-negativity of $T_m(\cdot)$ and (49) yields

$$\Lambda_m^{(m,m)}(\beta) = \frac{1}{\bar{\eta}_m - 1} \left(T_m(\Gamma(\beta)) \right)^{(1,1)} > 0.$$

Strict sub-homogeneity: For any $\alpha > 1$ and $\beta \in \mathbb{R}_+ \setminus \{0\}$, it is obvious from (16) that $\Gamma(\alpha\beta) \prec \alpha\Gamma(\beta)$. The strict monotonicity and homogeneity of $T_m(\cdot)$ together with (49) give

$$\begin{aligned} \Lambda_m^{(m,m)}(\alpha\beta) &= \frac{1}{\bar{\eta}_m - 1} \left(T_m(\Gamma(\alpha\beta)) \right)^{(1,1)} \\ &< \frac{1}{\bar{\eta}_m - 1} \left(T_m(\alpha\Gamma(\beta)) \right)^{(1,1)} \\ &= \frac{\alpha}{\bar{\eta}_m - 1} \left(T_m(\Gamma(\beta)) \right)^{(1,1)} \\ &= \alpha \Lambda_m^{(m,m)}(\beta). \end{aligned}$$

Monotonicity: For any $\beta_1, \beta_2 \in \mathbb{R}_+^K$ with $\beta_1 \geq \beta_2$, we have $\Gamma(\beta_1) \succeq \Gamma(\beta_2)$ by (16). By the monotonicity of $T_m(\cdot)$ and (49), we have

$$\begin{aligned} \Lambda_m^{(m,m)}(\beta_2) &= \frac{1}{\bar{\eta}_m - 1} \left(T_m(\Gamma(\beta_2)) \right)^{(1,1)} \\ &\leq \frac{1}{\bar{\eta}_m - 1} \left(T_m(\Gamma(\beta_1)) \right)^{(1,1)} \\ &= \Lambda_m^{(m,m)}(\beta_1). \end{aligned}$$

□

B. Useful Properties of $\mathbf{Q}(\cdot)$

We have the following lemma about the useful properties of $\mathbf{Q}(\cdot)$ given by (27)–(29).

Lemma 6: The mapping $\mathbf{Q}(\cdot)$ given by (27)–(29) is non-negative, linear, and monotonic.

Proof: It suffices to show the linearity and non-negativity of $\mathbf{Q}(\cdot)$ since the monotonicity of $\mathbf{Q}(\cdot)$ automatically follows from these two properties using Lemma 3. In the following, we show these two properties of $\mathbf{Q}(\cdot)$ by induction.

It is obvious that $\mathbf{Q}^{(M,M)}$ given in (27) is non-negative and linear. Suppose $\mathbf{Q}^{(m+1:M, m+1:M)}$ is non-negative and linear. First, by (28) and (29), $\mathbf{Q}^{(m+1:M, m)}$ and $\mathbf{Q}^{(m, m)}$ is linear. Combining this with the assumption shows the linearity of $\mathbf{Q}^{(m:M, m:M)}$. Next, by the elementary properties of the Schur complements [48, Theorem 1.20], to show the non-negativity of $\mathbf{Q}^{(m:M, m:M)}$, it suffices to check the following two conditions.

- (i) $\mathbf{Q}^{(m:M, m:M)} / \mathbf{Q}^{(m+1:M, m+1:M)}$ is non-negative; and
- (ii) for any $\mathbf{x} \in \mathbb{C}^{M-m-2}$ with $\mathbf{Q}^{(m+1:M, m+1:M)} \mathbf{x} = \mathbf{0}$, we have $\mathbf{Q}^{(m, m+1:M)} \mathbf{x} = \mathbf{0}$.

Plugging (28) and (29) into expressions in the above (i) and (ii), we have

$$\begin{aligned} &\mathbf{Q}^{(m:M, m:M)} / \mathbf{Q}^{(m+1:M, m+1:M)} \\ &= \frac{1}{\bar{\eta}_m - 1} \left(\frac{\lambda_m^{(m+1:M)\dagger} \mathbf{Q}^{(m+1:M, m+1:M)} \lambda_m^{(m+1:M)}}{|\lambda_m^{(m)}|^2} \right. \\ &\quad \left. + \sum_{k \in \mathcal{K}} p_k \hat{\mathbf{V}}_k^{(m, m)} \right) \geq 0; \end{aligned} \quad (51)$$

and for any $\mathbf{x} \in \mathbb{C}^{M-m-2}$ with $\mathbf{Q}^{(m+1:M, m+1:M)} \mathbf{x} = \mathbf{0}$, we have

$$\mathbf{Q}^{(m, m+1:M)} \mathbf{x} = \frac{\lambda_m^{(m+1:M)\dagger} \mathbf{Q}^{(m+1:M, m+1:M)} \mathbf{x}}{\lambda_m^{(m)\dagger}} = \mathbf{0}. \quad (52)$$

Hence, we get the non-negativity of $\mathbf{Q}^{(m:M, m:M)}$. It follows by induction that $\mathbf{Q}^{(m:M, m:M)}$ is non-negative and linear for any $m \in \mathcal{M}$. Taking $m = 1$, we obtain the desired result. □